Title
Engineering the Synthesis of Five-Carbon Alcohols from Isopentenyl Diphosphate and Increasing its Production Using an Adaptive Control System

Author
Chou, Howard

Publication Date
2012

Peer reviewed|Thesis/dissertation

Engineering the Synthesis of Five-Carbon Alcohols from Isopentenyl Diphosphate and Increasing its Production Using an Adaptive Control System

By

Howard H. Chou

A dissertation submitted in partial satisfaction of the

requirements for the degree of

Joint Doctor of Philosophy

with the University of California, San Francisco

in

Bioengineering

in the

Graduate Division

of the

University of California, Berkeley

Committee in charge:

Professor Jay D. Keasling, Chair

Professor Adam P. Arkin

Professor Patricia Babbitt

Professor John Coates

Fall 2012

Engineering the Synthesis of Five-Carbon Alcohols from Isopentenyl Diphosphate and Increasing its Production Using an Adaptive Control System

Abstract

Engineering the Synthesis of Five-Carbon Alcohols from Isopentenyl Diphosphate and Increasing its Production Using an Adaptive Control System

by

Howard H. Chou

Joint Doctor of Philosophy in Bioengineering

University of California, Berkeley

and

University of California, San Francisco

Professor Jay D. Keasling, Chair

Concerns over the sustainability and environmental impact of current processes that rely heavily on nonrenewable petroleum feedstock have created a need for developing alternative processes. Bioprocesses that use enzymes or whole cells to transform renewable biomass feedstock into commercial products are an alternative that could be more sustainable and environmentally friendly. Here, I present three novel frameworks for designing, assembling, and optimizing biological pathways that could be utilized in bioprocesses. The first framework uses enzyme families as libraries for identifying enzymes able to catalyze novel reactions. I used the framework to assemble a synthetic biological pathway that produces 3-methyl-3-butenol, 3-methyl-2-butenol, and 3-methyl-butanol from isopentenyl diphosphate. I also developed a novel colorimetric assay using N-methylbenzothiazolinone-2-hydrazone to rapidly quantify these three five-carbon alcohols. The second framework is called feedback-regulated evolution of phenotype (FREP), and describes a system that dynamically regulates the mutation rate in the cell based on the level of a particular phenotype. I used the FREP framework to engineer increased tyrosine production in *Escherichia coli*. Finally, the third framework describes the construction of synthetic transcription factors using metabolic enzymes. I used the framework to assemble four different transcription factors, all of which generate a transcriptional change as a result of a change in isopentenyl diphosphate concentration. By combining the FREP and synthetic transcription factor assembly frameworks, I implemented an adaptive control system that increased isopentenyl diphosphate production in *Escherichia coli*.

Table of Contents

Chapter 1: Introduction

The chemical and transportation industries currently use nonrenewable petroleum feedstock to produce commercially important products, such as fuels, materials, and pharmaceuticals. However, concerns over the environmental impact and possible effects on global warming of these traditional processes raise questions about their sustainability, especially as emerging economies continue to increase their rate of consumption of petroleum-derived products. Dramatic fluctuations in the price of crude oil have also led to the development of new processes in the oil industry that are potentially even more harmful to the environment, such as deepwater drilling, hydraulic fracturing, and various methods used to extract crude oil from oil sands. As a result, there are many ongoing efforts to develop more sustainable practices that are able to produce commercially important products from renewable resources.

One such effort is the use of bioprocesses to produce commercial products from renewable carbon sources, such as lignocellulosic biomass. Lignocellulosic biomass represents an abundant source of currently unused carbon that is found as agricultural and forestry residues, the organic fraction of municipal solid waste, and the waste stream of industrial processing residues from the paper and pulp industry. The composition of lignocellulosic biomass is typically 35-50% cellulose, 20-35% hemicellulose, and 15-25% lignin (1). Cellulose is a polymer of glucose, while hemicellulose is a polymer consisting of mainly xylose and arabinose. Using fermentation, these sugar monomers could be converted into chemicals that could either substitute or replace chemicals already produced from petroleum. We have proposed several biological pathways for making industrial chemicals, including biofuel (2, 3, 4).

The transition from traditional processes that use petroleum feedstock to bioprocesses that use lignocellulosic biomass feestock faces two major challenges: development of new biological processes to produce commercial products, and the optimization of those processes to make them commercially viable. In this dissertation, I describe three frameworks for tackling these two challenges. Chapter 2 illustrates a framework that uses enzyme families as libraries to indentify enzymes able to catalyze a desired novel reaction in order to assemble synthetic biological pathways. I used the framework to construct a novel synthetic pathway (5) that converts isoprenyl diphosphate (IPP) into three different five-carbon alcohols: 3-methyl-3-butenol, 3-methyl-2-butenol, and 3-methyl-butanol. A new colorimetric assay for rapidly quantifying five-carbon alcohol production is presented in Chapter 3.

Chapter 4 describes two frameworks. The first is for constructing synthetic transcription factors from metabolic enzymes. The second is for implementing an adaptive control system that dynamically regulates the mutation rate in a cell based on the level of a target phenotype called feedback-regulated evolution of phenotype (FREP). Previously, I engineered AraC to be less sensitive to isopropyl β-D-1-thiogalactopyranoside (6). Here, I used the synthetic transcription factor assembly framework to transform AraC into a bacterial transcription factor that recognizes IPP instead of arabinose, and constructed three additional yeast transcription factors capable of recognizing IPP. I combined the

new AraC-based IPP transcription factor with the FREP framework in order to engineer the evolution of increased IPP production in *Escherichia coli*.

Chapter 2: Synthetic Pathway to Produce Five-Carbon Alcohols from Isopentenyl Diphosphate

Abstract

Synthetic biological pathways could enhance the development of novel processes for producing chemical building blocks from renewable resources. Based on models describing the evolution of metabolic pathways and enzymes in nature, we developed a framework to rationally identify enzymes able to catalyze unnatural reactions, overcoming one of the major bottlenecks in assembling a synthetic biological pathway. We verified the framework by implementing a synthetic pathway with two novel enzymatic reactions to convert isopentenyl diphosphate into 3-methyl-3-butenol, 3-methyl-2-butenol, and 3-methyl-butanol. To overcome competition with native pathways sharing the same substrate, we engineered two new bifunctional enzymes to redirect metabolic flux towards the synthetic pathway. Taken together, our work demonstrates a new approach to engineering novel catalytic reactions in the cell.

Introduction

The chemical and transportation industries currently use limited nonrenewable resources to produce raw materials that could instead be synthesized from renewable resources using metabolic engineering (7). Natural biological pathways have traditionally been the source of industrially important chemicals produced using fermentation (8). Some of the regulatory mechanisms limiting production in the native hosts are circumvented by reconstructing pathways in heterologous hosts (9,10). To synthesize chemicals not produced by natural pathways, enzymes are over-expressed in novel combinations in order to construct synthetic biological pathways (11, 12, 13, 14, 15).

One of the rate-limiting steps in assembling a synthetic pathway is identifying enzymes that are capable of catalyzing new reactions of interest. Although relying on known natural enzymatic reactions limits the number of synthetic pathways that could be assembled, the task of engineering an enzyme to catalyze a novel reaction remains challenging. Strategies that incorporate directed evolution or metagenomic libraries require product-specific high-throughput screens or selections in order to identify enzymes able to catalyze a desired reaction (16). Rational and *in silico* protein engineering strategies generate smaller libraries to alleviate the need for high-throughput technologies, but require *a priori* knowledge about the protein being engineered (17). Therefore, the effort to engineer a new reaction in a cell is often hindered by the lack of high-throughput screens or selections, and insufficient knowledge about how to rationally engineer a protein to catalyze the desired reaction.

We describe a new framework that is built on theoretical models of pathway and enzyme evolution for identifying proteins able to catalyze reactions not found in nature. One of the models describing natural pathway evolution suggests that a new biological pathway

is assembled by recruiting enzymes from existing pathways (18). As a result, the enzymes that are recruited often evolve altered substrate specificities while retaining their fundamental chemical capabilities (19). We hypothesized that an enzyme family (20), as a collection of evolutionarily related proteins with functional conservation, could be regarded as a library of enzymes able to catalyze a specific chemistry on various substrates. These libraries might provide an organism with a pool of enzymes from which to quickly evolve new reactions and pathways that might be useful for example during adaptation to xenobiotics (21). The cell's ability to assemble new pathways is further facilitated by the high degree of substrate promiscuity demonstrated by some enzymes (22, 23).

We reasoned enzyme families could also be used in the laboratory to assemble synthetic biological pathways in order to develop new processes for converting biomass to biofuels and biomaterials in a cell. As an example, we chose to develop a metabolic pathway to produce 3-methyl-butanol, 3-methyl-3-butenol, and 3-methyl-2-butenol, which have better combustion efficiencies and more similar research octane numbers (RONs; 102, 102, and 92, respectively) to gasoline than ethanol, which is widely used as a gasoline oxygenate and substitute (24, 25). 3-Methyl-2-butenol can be readily converted to citral, an intermediate in the synthesis of pharmaceuticals, vitamin A, vitamin E, some widely-used carotenoids, and certain flavors and fragrances (26). 3-Methyl-butanol has been produced in *Escherichia coli* (27) modified with the Ehrlich pathway (28) from *Saccharomyces cerevisiae*, but no pathway exists to synthesize either 3-methyl-3-butenol or 3-methyl-2-butenol. Using enzyme families as libraries to screen for novel enzymatic reactions, we explored *E. coli*'s metabolic potential and assembled a synthetic pathway to produce 3-methyl-butanol, 3-methyl-3-butenol, and 3-methyl-2-butenol from isopentenyl diphosphate (IPP), the central metabolite in isoprenoid biosynthesis (29), from only *E. coli* enzymes. This pathway has the advantage of being able to build on previous work (30, 31) in engineering the isoprenoid pathway to more quickly improve production titers in the future.

Materials and Methods

Oligonucleotides and DNA sequencing. All oligonucleotides were obtained from Integrated DNA Technologies with standard purification. Primer sequences mentioned here are presented in Appendix A.1. DNA sequencing to confirm cloning products was performed by Quintara Biosciences.

Strains and plasmids availability. Strains, plasmids, and plasmid sequences (in Genbank format) constructed in this study are deposited in the private instance of the JBEI registry and will be moved to the public instance (https://public-registry.jbei.org) after publication. Strains and plasmids are physically available from Addgene (http://www.addgene.org).

Strains. All of the experiments were performed in either *E. coli* JM109 or DH1. All genes amplified from *E. coli* were from MG1655.

Construction of plasmids for phosphatase and reductase libraries. pHADX (where X is a number from 1 to 23) were constructed by amplifying *had*X from the *E. coli* chromosome using the primers HADX-F and HADX-R, and cloning into pTrc99A using NcoI and EcoRI. pNUDY (where Y is a letter from A to M) were constructed by amplifying *nud*Y from the *E. coli* chromosome using the primers NUDY-F and NUDY-R, and cloning into pTrc99A using NcoI and EcoRI. pNemA was constructed by amplifying *nemA* from the *E. coli* chromosome using the primers NEMA-F and NEMA-R, and cloning into pTrc99A using EcoRI and KpnI. PCR, restriction digest, and ligation reactions were performed using standard cloning protocols following the manufacturers' instructions.

Screening for enzymes able to catalyze the phosphatase reaction. pHADX (where X is a number from 1 to 23) and pNUDY (where Y is a letter from A to M) were transformed into *E. coli* JM109 co-expressing pMevT and pMevB (9), and plated on LB agar plates with ampicillin, chloramphenicol, and tetracycline. 3-Methyl-3-butenol production was analyzed using GC-MS.

Screening for enzymes able to catalyze the reductase reaction. pNemA was transformed into *E. coli* DH1, and plated on LB agar plates with ampicillin. Growth and experimental protocols were the same as other experiments except 1 g/L of 3-methyl-2-butenol was added to the medium after induction with isopropyl β-D-1-thiogalactopyranoside (IPTG) (Sigma-Aldrich). 3-Methyl-butanol production was analyzed using GC-MS.

Protein purification of NudB and in vitro assay for phosphatase activity. We amplified NudB using the primers NUDB-F and NUDB-R3 from pNUDB, and cloned the PCR product into pPro29b (32) using NcoI and BamHI to make pPro29b-NUDB. *E. coli* BLR(DE3) was transformed with pPro29b-NudB, and an overnight culture was inoculated into a liter of LB medium with ampicillin to an initial Abs_{600} of 0.05. We grew the culture at 37°C until the Abs_{600} reached 0.6, induced it with 20 mM propionate, and grew it overnight at 20°C. The cells were pelleted, resuspended in binding buffer (50 mM Tris-HCl, pH 7.5, 1 mM EDTA, 0.1 mM dithiothreitol), sonicated, and centrifuged. The tagged protein was purified from the supernatant using the S•Tag Thrombin Purification Kit (Novagen) following the manufacturer's instructions. Protein concentration was determined using the Pierce BCA Protein Assay Kit (Thermo Scientific).

The standard reaction mixture for studying NudB kinetics contained the following in 100 µL: 50 mM Tris, pH 8.0, 10 mM $MgCl_2$, 1 mM DTT, 200 µM 7-methylguanosine (7-MEG) (Sigma-Aldrich), 0.5 U/mL bacterial purine nucleoside phosphorylase (PNPase) (Sigma-Aldrich), 0.5 U/mL yeast inorganic pyrophosphatase (PPase) (Sigma-Aldrich), and 0.5 µM Phosphate Sensor (Invitrogen). Phosphate release was measured using a Spectramax M2 (Molecular Devices) exciting at 426 nm and measuring emission at 464 nm. A standard curve comparing the concentration of P_i to fluorescence was made by incubating different concentrations of P_i to the standard mixture.

To determine NudB kinetics, 15 different concentrations of isopentenyl pyrophosphate triammonium salt solution (IPP salt) (Sigma-Aldrich) ranging from 0 to 25 μM were tested. The assay was performed at 30°C with 10 mM of purified NudB, and IPP salt was added to start the reaction. The reaction was monitored in a Spectramax M2 for 3 minutes, and the change in fluorescence was used to calculate the velocity of the reaction after being normalized to the sample with 0 μM IPP salt. The change in fluorescence was converted to a change in P_i concentration using the standard curve. SigmaPlot and its Enzyme Kinetics module was used to analyze the velocity data to calculate V_{max} and K_m.

Construction of fusion proteins Idi-NudB and Idi1-NudB. The gene for Idi was amplified from the *E. coli* chromosome using the primers IDI-F2 and IDI-NUDB-SOE-R, and the gene for NudB was amplified using the primers IDI-NUDB-SOE-F and NUDB-R2. The PCR products were used as templates in a second PCR with the primers IDI-F2 and NUDB-R2 to amplify the fusion protein Idi-NudB, which was cloned into pTrc99A using EcoRI and KpnI to construct pIdi-NudB. pIdi1-NudB was constructed similarly, except Idi1 was amplified from the *S. cerevisiae* chromosome using the primers IDI1-F and IDI1-NUDB-SOE-R, NudB was amplified using the primers IDI1-NUDB-SOE-F and NUDB-R2, and Idi1-NudB was amplified using IDI1-F and NUDB-R2 in the second PCR. The 19- and 15-amino acid linkers used to construct Idi-NudB and Idi1-NudB, respectively, were based on previous work (33).

Construction of plasmids with isomerase, phosphatase, and reductase activities. *idi* was amplified from the *E. coli* chromosome using the primers IDI-F and IDI-R, and cloned using EcoRI and KpnI into pTrc99A and pNudB to construct pIdi and pNudB-s-Idi, respectively. *nemA* was amplified from pNemA using the primers NEMA-F2 and NEMA-R2, and cloned using BamHI and XbaI into pIdi-NudB to construct pIdi-NudB-s-NemA. *nemA* was amplified from pNemA using the primers NEMA-F3 and NEMA-R2, and cloned using BamHI and XbaI into pIdi1-NudB to construct pIdi1-NudB-s-NemA.

Verification of IPP conversion to 3-methyl-2-butenol and 3-methyl-butanol. pIdi, pNudB-s-Idi, pIdi-NudB, pIdi1-NudB, pIdi-NudB-s-NemA, and pIdi1-NudB-s-NemA were transformed into *E. coli* JM109 co-expressing pMevT and pMevB (9), and plated on LB agar plates with ampicillin, chloramphenicol, and tetracycline. 3-methyl-3-butenol, 3-methyl-2-butenol, and 3-methyl-butanol production were analyzed using GC-FID.

Growth and GC protocols for production and detection of C5 Alcohols. Three colonies were picked for each construct and grown overnight at 37°C in 5 mL of LB medium with antibiotic. The overnight cultures were inoculated into 5 mL of EZ Rich Defined Medium (Teknova) with 0.2% glucose and antibiotic to an initial Abs_{600} of 0.05. Cultures were grown at 37°C for 3 hours, induced with 0.5 mM IPTG, and grown for 20 hours at 30°C. 700 μL of culture was sampled, mixed with a solvent of chloroform:methanol (80:20) spiked with 50 μg/mL of butanol (Sigma-Aldrich) as an internal standard, vortexed for 15 minutes, and centrifuged for 1 minute at 13,000 × g. The chloroform layer was removed for analysis on a GC.

The GC-MS data were collected in full-scan mode (m/z 50-300) using a Tr-Wax column (0.25 mm x 30 m, 0.25 μm film thickness; Thermo Electron) on a PolarisQ GC-MS with TriPlus autosampler (Thermo Electron). The carrier flow was 1.2 ml min^{-1}, and the inlet temperature was set to 200°C. The oven program was as follows: 40°C (1.20 min hold), 40-130°C (25°C min^{-1}), 130-220°C (35°C min^{-1}). The solvent delay was set at 3.40 min. Samples were normalized using the butanol internal standard and quantified using authentic standards. 3-Methyl-butanol standards were purchased from Sigma-Aldrich. 3-Methyl-3-butenol and 3-methyl-2-butenol were purchased from Tokyo Chemical Industry.

The GC-FID data were collected using a Tr-Wax column (0.25 mm x 30 m, 0.25 μm film thickness; Thermo Electron) on a Focus GC with TriPlus autosampler (Thermo Electron). The carrier was set at constant pressure for 300 kPa, and the inlet temperature was set to 200°C. The oven program was as follows: 40°C (1.50 min hold); 40-110°C (15°C min^{-1}). Samples were normalized using the butanol internal standard and quantified using authentic standards.

Results

A synthetic pathway converts IPP into three five-carbon alcohols. IPP is naturally synthesized using either the mevalonate or deoxyxylulose 5-phosphate (DXP) pathway, and is the primary substrate of the synthetic biological pathway (Fig. 1). Three enzymatic reactions could convert IPP into three C5 alcohols: 3-methyl-3-butenol, 3-methyl-2-butenol, and 3-methyl-butanol. Reaction 1 isomerizes IPP to dimethylallyl pyrophosphate (DMAPP). Reaction 2 dephosphorylates IPP and DMAPP to produce 3-methyl-3-butenol and 3-methyl-2-butenol, respectively. Reaction 3 reduces 3-methyl-2-butenol to produce 3-methyl-butanol. Reaction 1 could be catalyzed by an enzyme with IPP isomerase activity. No natural enzymes are known to catalyze either Reaction 2 or 3, so we identified three enzyme families to screen for enzymes that might catalyze these novel reactions.

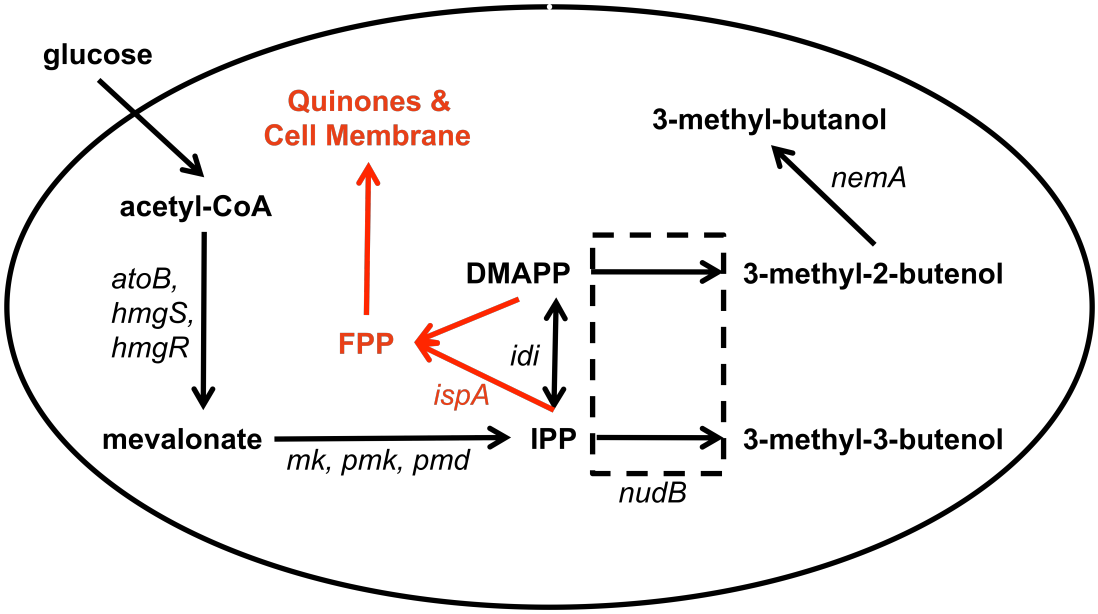

Fig. 1. Synthetic pathway converts isopentenyl diphosphate (IPP) to 3-methyl-3-butenol, 3-methyl-2-butenol, and 3-methyl-butanol. IPP is produced by co-expressing the mevalonate pathway genes (*atoB*, *hmgS*, *hmgR*, *mk*, *pmk*, *pmd*) in *E. coli*. Three different reactions could convert IPP into three different 5C alcohols. Reaction 1 catalyzes the isomerization of IPP to dimethylallyl diphosphate (DMAPP). Reaction 2 catalyzes the dephosphorylation of IPP into 3-methyl-3-butenol and DMAPP into 3-methyl-2-butenol. Reaction 3 catalyzes the reduction of 3-methyl-2-butenol to 3-methyl-butanol. The synthetic pathway competes with native pathways in *E. coli* that also use IPP and DMAPP as substrates, such as those for quinone and cell membrane synthesis (shown in red).

IPP phosphatase activity is discovered by screening two enzyme families. We identified the haloacid dehalogenase (HAD) (34) and Nudix hydrolase (35) superfamilies as likely to contain enzymes capable of catalyzing the dephosphorylation of IPP and DMAPP. The prevalence of both superfamilies in all three domains of life (bacteria, archaea, and eukaryotes) suggests that their members are used extensively throughout evolution to catalyze mechanistically diverse reactions on various substrates (36). We limited our search to the family of 23 HAD-like phosphatases in *E. coli* (37) within the HAD superfamily as the first library, and the family of 13 phosphatases in *E. coli* (38) within the Nudix superfamily as the second library.

We screened the two libraries of small molecule phosphatases for the ability to catalyze the conversion of IPP to 3-methyl-3-butenol by overexpressing each enzyme in *E. coli* harboring the mevalonate pathway genes. Successful catalysis of Reaction 2 was determined by detecting 3-methyl-3-butenol production using gas chromatography (GC). Out of the thirty-six enzymes screened, overexpression of two HAD-like phosphatases (HAD4 and HAD10) and five Nudix hydrolases (NudB, NudF, NudI, NudJ, NudM) led to a more than two-fold increase in production of 3-methyl-3-butenol compared to the negative control not overexpressing any protein (Fig. 2). NudF, whose isozyme from *Bacillus subtilis* was identified to have prenyl alcohol biosynthesis activity (39), demonstrated an almost three-fold improvement in production over the negative control.

The overexpression of NudB led to the greatest conversion of IPP to 3-methyl-3-butenol *in vivo*, producing five-fold more C5 alcohol than the negative control.

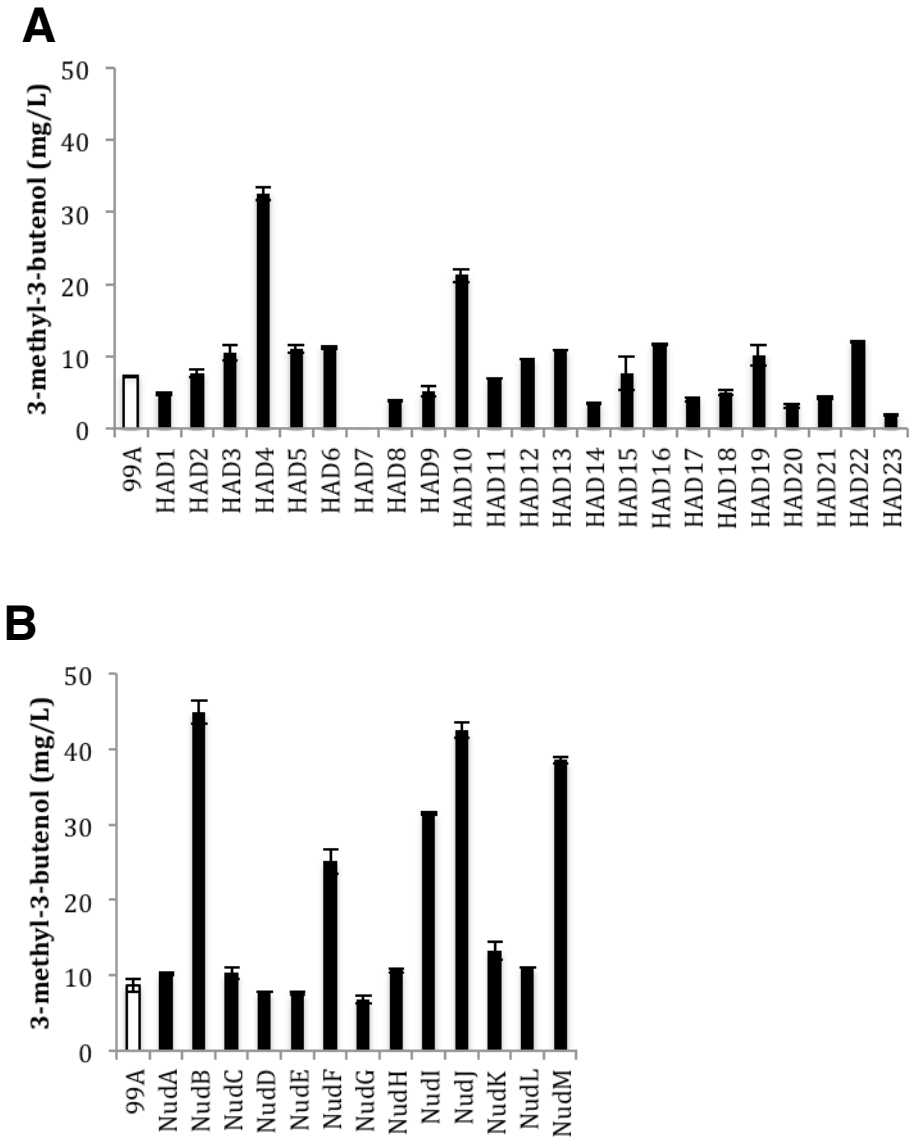

Fig. 2. Enzymes catalyzing Reaction 2 are identified from two libraries. (**A**) The family of 23 haloacid dehalogenase (HAD)-like phosphatases from *E. coli* (black bars) was screened for an enzyme able to catalyze the dephosphorylation of IPP to 3-methyl-3-butenol. Overexpression of HAD4 and HAD10 led to a more than two-fold increase in 3-methyl-3-butenol production compared to the negative control (white bar). (**B**) The family of 13 Nudix hydrolases from *E. coli* (black bars) was screened for an enzyme able to catalyze the dephosphorylation of IPP to 3-methyl-3-butenol. Overexpression of NudB, NudF, NudI, NudJ, and NudM led to a more than two-fold increase in 3-methyl-3-butenol production compared to the negative control (white bar).

IPP phosphatase activity is verified in vitro. We verified NudB's ability to catalyze Reaction 2 *in vitro* by developing an assay for detecting the phosphatase reaction with IPP as a substrate. The assay measures pyrophosphate release kinetics in real-time using

a coupled enzyme assay that produces a fluorescent output (40). We determined the V_{max} of NudB to be 0.63 nmole/min/mg and its K_m to be 4.7 μM for IPP (Fig. 3). NudB's K_m is comparable to that of *E. coli* IPP isomerase Idi, but its V_{max} is 1000-fold less than that of Idi (41). The poor kinetics of NudB for IPP exemplifies the natural evolution of an enzyme, which generally begins with a protein having low affinity for a new substrate or low rates of catalytic action on the bound substrate (42). Overall, the *in vitro* data support the *in vivo* data that NudB binds IPP and catalyzes the phosphatase reaction to convert it to 3-methyl-3-butenol.

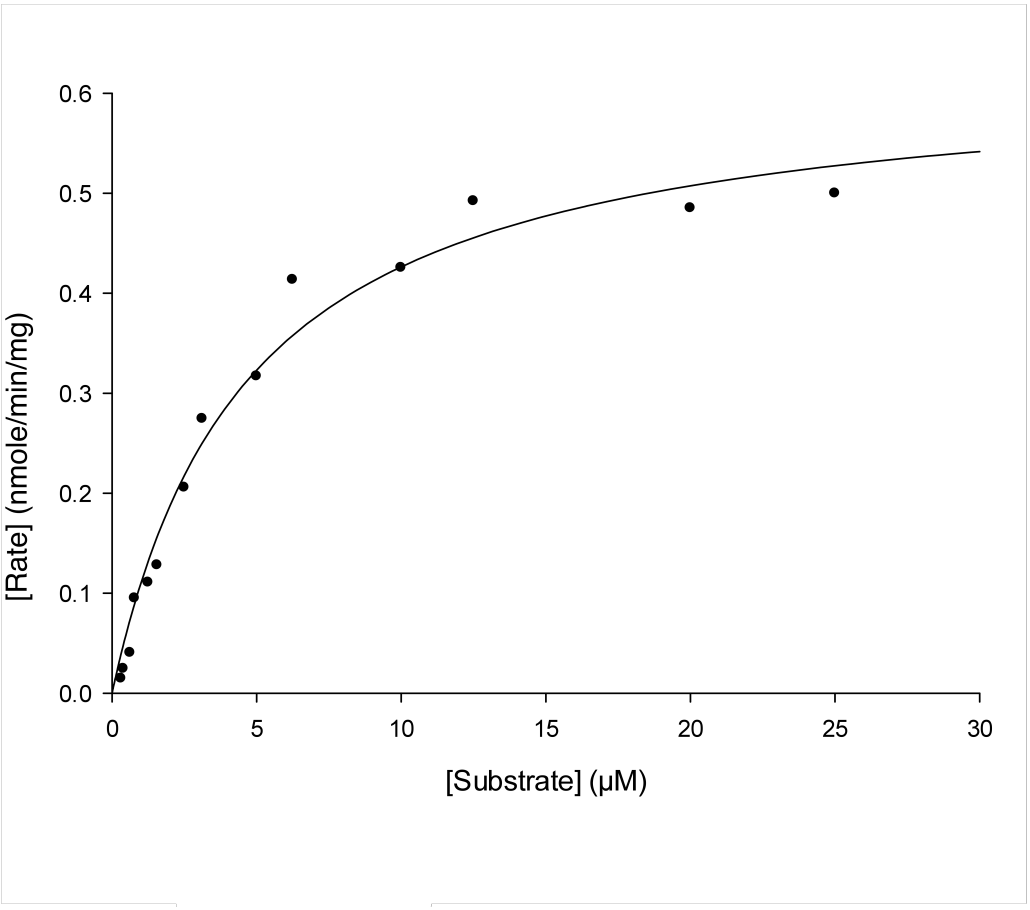

Fig 3. NudB kinetics. An in vitro assay was developed to monitor the dephosphorylation of IPP by NudB. The K_m of the NudB phosphatase reaction on IPP is 4.7 uM and its Vmax is 0.6264. The R^2 is 0.97. Each data point is the average of three replicates.

3-methyl-2-butenol reductase activity is discovered from one enzyme family. We identified the Old Yellow Enzyme (OYE) family (43) as likely to contain enzymes able to catalyze the reduction of 3-methyl-2-butenol to 3-methyl-butanol. The OYE family is represented in both prokaryotes and eukaryotes, and several members are associated with xenobiotic metabolism (44), suggesting that natural systems exploit the propensity of these enzymes to catalyze novel reactions. We limited our search to the OYE family in *E. coli* capable of reducing α/β-unsaturated carbonyl functionalities.

NemA (45), the only documented member of the OYE from *E. coli* that fit our criteria, was overexpressed in the presence of 1 g/L of 3-methyl-2-butenol in the medium, and catalysis of Reaction 3 was confirmed by measuring 3-methyl-butanol production using GC. The overexpression of NemA led to 3-methyl-butanol production, and the conversion of 3-methyl-2-butenol to 3-methyl-butanol was 40% after 24 hours (Fig. 4). The negative control that did not overexpress any enzyme did not produce any 3-methyl-butanol. Even though 3-methyl-2-butenol lacks the α/β-unsaturated carbonyl functional group present in most of the substrates of enzymes in the OYE family, overexpression of NemA demonstrated increased 3-methyl-butanol production from 3-methyl-2-butenol. The data suggest that promiscuous oxidases and reductases in *E. coli* might be acting in concert with NemA and generating the aldehyde intermediates necessary for catalyzing Reaction 3, and the activities of these auxiliary enzymes are sufficient for 3-methyl-butanol production to be observed.

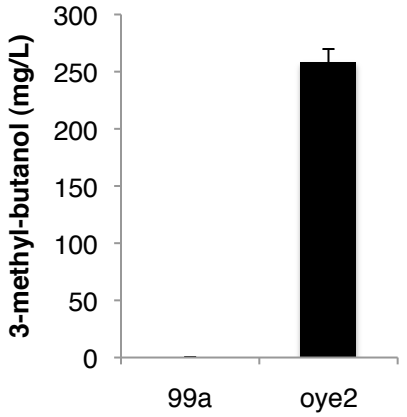

Fig. 4. An enzyme catalyzing Reaction 3 is identified. NemA of the Old Yellow Enzyme family from *E. coli* was overexpressed in the presence of 1 g/L 3-methyl-2-butenol. After 24 hours, 40% of the 3-methyl-2-butenol was converted to 3-methyl-butanol. No production of 3-methyl-butanol was observed in the negative control.

Idi-NudB fusion overcomes competition with native pathways for IPP and DMAPP. We overexpressed *E. coli* IPP isomerase (Idi) to catalyze Reaction 1 and NudB to catalyze Reaction 2 in *E. coli* harboring the mevalonate pathway in order to synthesize 3-methyl-2-butenol from IPP. However, co-expression of Idi and NudB decreased 3-methyl-3-butenol production by five fold compared to overexpression of NudB by-itself, and no 3-methyl-2-butenol production was observed (Fig. 5A). No 3-methyl-3-butenol or 3-methyl-2-butenol production was observed when Idi was overexpressed by-itself. We reasoned that the IPP and DMAPP produced by the heterologous mevalonate pathway were consumed by native enzymes, since *in vitro* analysis of NudB indicated it is relatively slow at catalyzing the new phosphatase reaction. For example, *E. coli* farnesyl pyrophosphate (FPP) synthase IspA (46) uses IPP and DMAPP to synthesize FPP, which is used in quinone and cell wall biosynthesis.

We hypothesized that a novel protein to restore 3-methyl-3-butenol production and synthesize 3-methy-2-butenol from IPP could be engineered by fusing Idi and NudB

together joined by a peptide linker to construct a single bifunctional polypeptide (Idi-NudB). Idi-NudB consists of two functional domains each catalyzing a different reaction (isomerization and dephosphorylation) that are parts of a consecutive reaction (conversion of IPP to DMAPP and DMAPP to 3-methyl-2-butenol). This fusion protein mimics natural bifunctional enzymes, such as *Arabidopsis* lysine-ketoglutarate reductase/saccharopine dehydrogenase (47), human 5-amino-4-imidazolecarboxamide ribonucleotide transformylase/inosine 5'-monophosphate cyclohydrolase (48), *Abies grandis* abietadiene synthase (49), and lysine-ketoglutarate reductase/saccharopine dehydrogenase from developing soybean seeds (50). We joined Idi and NudB with a peptide linker, because linkers can control favorable and unfavorable interactions between adjacent protein domains (51).

The overexpression of the Idi-NudB fusion increased C5 alcohol production by more than two-fold compared to overexpressing Idi and NudB separately, and led to 3-methyl-2-butenol production (Fig. 5B). We constructed a variant of Idi-NudB by fusing the *S. cerevisiae* IPP isomerase Idi1 (52) to NudB (Idi1-NudB). The overexpression of Idi1-NudB increased 3-methyl-3-butenol and 3-methyl-2-butenol production by 40% compared to Idi-NudB. The mevalonate pathway only produces IPP, and the DXP pathway produces IPP and DMAPP in a 6:1 ratio (53). Regardless of the production pathway, the intracellular ratio of IPP to DMAPP is 1:2.5 in the presence of IPP isomerase (54). We observed a ratio of 3-methyl-3-butenol to 3-methyl-2-butenol produced by Idi-NudB and Idi1-NudB to be 2:1, suggesting that either the catalytic activity of IPP isomerase is altered when it is fused to NudB or the fusion proteins prefer to dephosphorylate IPP. The production of 3-methyl-2-butenol from IPP by the fusion proteins indicates that the catalytic domains of Idi and NudB are functional, the single polypeptides are bifunctional, and Idi-NudB and Idi1-NudB can compete with the native enzymes in *E. coli* for IPP and DMAPP.

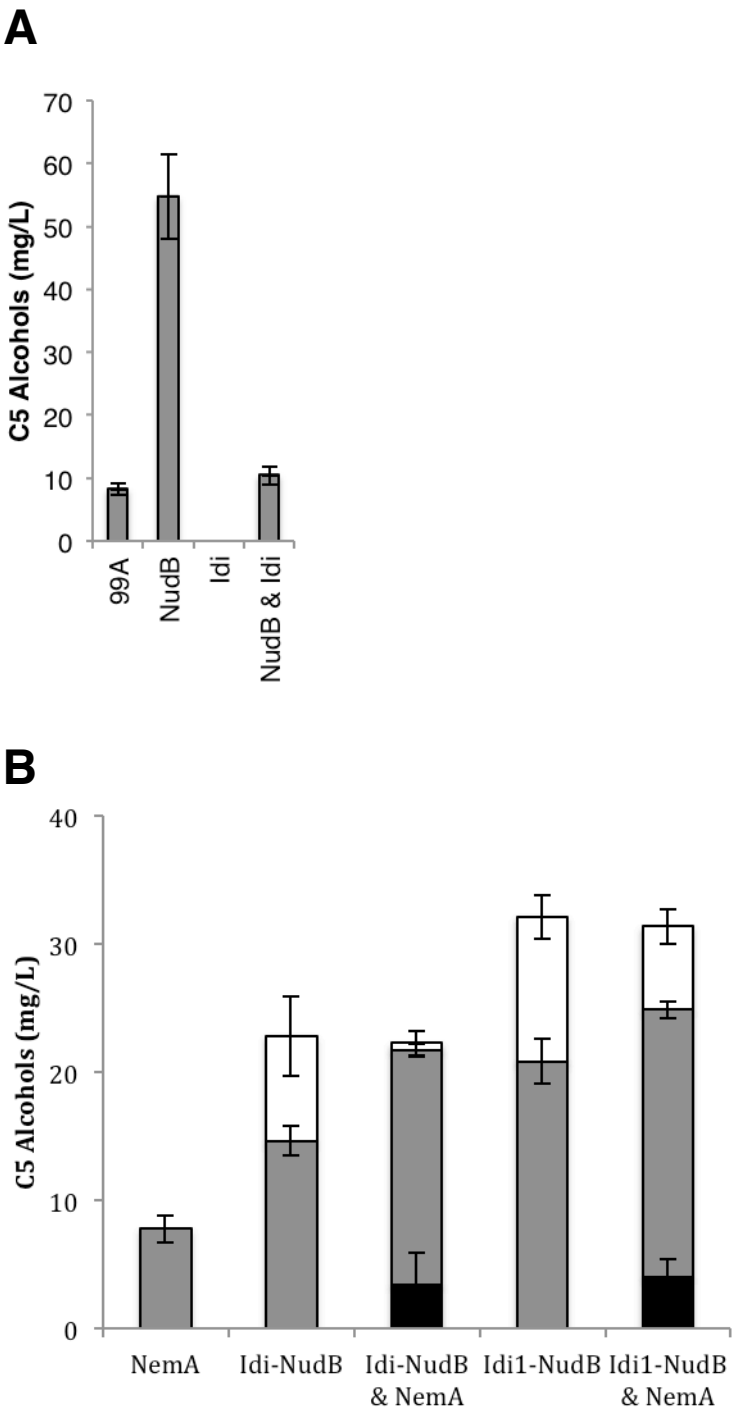

Fig. 5. 3-methyl-3-butenol, 3-methyl-2-butenol, and 3-methyl-butanol are produced from IPP. (**A**) No C5 alcohol production was observed when Idi was overexpressed by-itself compared to the negative control (99A) and positive control (NudB). Co-expression of NudB and Idi produced five fold less 3-methyl-3-butenol (gray bars) than the positive control. (**B**) Overexpression of the fusion proteins Idi-NudB and Idi1-NudB increased C5 alcohol production by more than two fold compared to co-expression of NudB and Idi, and 3-methyl-2-butenol production (white bars) was observed. Production of 3-methyl-butanol (black bars) was observed

by co-expressing NemA with either Idi-NudB or Idi1-NudB. No production of either 3-methyl-2-butenol or 3-methyl-butanol was observed when only NemA was overexpressed.

Three five-carbon alcohols are produced from IPP. We assembled the entire synthetic pathway by overexpressing either i*di-nudB* or i*di1-nudB*, the protein product of which would catalyze Reactions 1 and 2, 5' of *nemA*, whose protein product would catalyze Reaction 3, to construct pIdi-NudB-s-NemA and pIdi1-NudB-s-NemA in *E. coli* harboring the genes in the mevalonate pathway, and observed production of 3-methyl-3-butenol, 3-methyl-2-butenol, and 3-methyl-butanol. The total amount of C5 alcohols produced remained the same compared to production in the absence of NemA, and the amount of 3-methyl-3-butenol remained unchanged. The decrease in 3-methyl-2-butenol production observed in the presence of NemA is accounted for by the increase in 3-methyl-butanol production. However, not all of the 3-methyl-2-butenol produced by Idi1-NudB was converted to 3-methyl-butanol, suggesting that *nemA* expression might be different when expressed 3' of Idi1-NudB compared to Idi-NudB, since less accumulation of 3-methyl-2-butenol was observed with Idi-NudB. The production of three 5C alcohols from IPP verifies our synthetic pathway and framework of using enzyme families to identify proteins able to catalyze new reactions.

Discussion

We assembled a synthetic pathway to produce 3-methyl-3-butenol, 3-methyl-2-butenol, and 3-methyl-butanol from IPP using a new framework that is based on theoretical models of pathway and enzyme evolution for rationally identifying enzymes that are able to catalyze reactions not found in nature. The framework is different from previous strategies for engineering synthetic pathways, because it does not rely on enzymes already known to catalyze each desired reaction. By rationally constructing small libraries of proteins using our framework, we identified enzymes able to catalyze two new reactions without the use of high-throughput technologies.

We screened thirty-six enzymes using GC and discovered seven with the novel phosphatase activity to convert IPP and DMAPP to 3-methyl-3-butenol and 3-methyl-2-butenol, respectively. An enzyme with a novel reductase activity to convert 3-methyl-2-butenol to 3-methyl-butanol was also discovered. All of the enzymes we used to construct the synthetic pathway (Idi, NudB, and NemA) are from *E. coli*, illustrating the catalytic and metabolic potential of this microorganism. Even though *E. coli* harbors all of the enzymes necessary to catalyze each separate reaction in the synthetic pathway, the poor kinetics of NudB for catalyzing the novel phosphatase reaction compared to the enzymes in the native pathways that consume IPP and DMAPP prevents any significant amounts of 3-methyl-3-butenol and 3-methyl-2-butenol from naturally accumulating.

By applying theories from protein evolution and dynamics, we also engineered two novel enzymes that successfully competed with native enzymes in *E. coli* for IPP and DMAPP. This approach to controlling metabolic flux in a new pathway complements existing metabolic engineering strategies based on controlling gene expression using gene knockouts, controlling plasmid copy number, and changing RBS or promoter strengths.

The overexpression of Idi-NuB and Idi1-NudB led to 3-methyl-2-butenol production, and the production of 3-methyl-butanol from IPP when they were co-expressed with NemA. This synthetic pathway provides a new process for producing 3-methyl-3-butenol, 3-methyl-2-butenol, and 3-methyl-butanol from IPP, and could build on previous engineering efforts that increased isoprenoid yields. The yields of these three 5C alcohols could also be increased by improving the catalytic efficiencies of the enzymes to perform the new reactions in the synthetic pathway using protein engineering, and balancing the enzymatic activities across the entire pathway using metabolic engineering.

The shift from nonrenewable to renewable resources for the synthesis of chemical building blocks used by various industries will require the invention of new processes to produce molecules that are functionally identical to those synthesized from nonrenewable resources. The field of synthetic chemistry facilitated the development of processes to produce novel compounds from basic laboratory materials. Similarly, metabolic engineering has the potential to produce novel compounds from renewable resources by engineering cells. To achieve that potential, new enzymes are necessary for assembling synthetic pathways, so that engineers are not limited to producing compounds from natural pathways nor reliant on known enzymatic reactions. The framework we describe here for discovering enzymes able to catalyze reactions not found in nature could be used to assemble a large number of synthetic biological pathways for producing chemicals with industrial applications.

Chapter 3: Colorimetric Assay for Quantifying Five-Carbon Alcohols

Abstract

The sizes of mutant enzyme libraries generated using established techniques typically exceed 10^3. However, 3-methyl-3-butenol, 3-methyl-2-butenol, and 3-methyl-butanol can only currently be detected using gas chromatography, which has a throughput of 10^2 samples/instrument/day. We have developed a new colorimetric assay to detect 3-methyl-3-butenol, 3-methyl-2-butenol, and 3-methyl-butanol that uses N-methylbenzothiazolinone-2-hydrazone. The assay can be performed at room temperature, takes less than an hour, and can be monitored at 620 nm. Using 96-well plates, the method could assay up to 10^4 samples/instrument/day. This assay enables mutants capable of increased 3-methyl-3-butenol, 3-methyl-2-butenol, and 3-methyl-butanol production to be screened in a high-throughput manner.

Introduction

As described in Chapter 2, 3-methyl-3-butenol, 3-methyl-2-butenol, and 3-methyl-butanol are potential biofuels and have industrial applications. Currently, the only method to detect these alcohols uses gas chromatography (GC). GC methods are relatively low throughput, can assay at most 10^2 samples/instrument/day, and involves costly materials and instruments. Directed evolution and rational protein engineering techniques have successfully increased the efficiency and expression of enzymatic processes (93). However, these techniques typically rely on the availability of high-throughput screens for the target molecules in order to identify useful mutants, because the number of mutants generated using these techniques can exceed 10^3. Therefore, screening mutants becomes one of the major bottlenecks for improving production.

A high-throughput screen is needed to detect 3-methyl-3-butenol, 3-methyl-2-butenol, and 3-methyl-butanol in order to take advantage of the directed evolution and protein engineering techniques that could be used to generate new strains demonstrating increased production of these alcohols. The alcohol group is a relatively unreactive functional group. Oxidation of the alcohol group into an aldehyde group would enable the use of several chromogens known to detect aldehydes, such as Purpald and N-methylbenzothiazolinone-2-hydrazone (MBTH). Purpald was used to identify Cytochrome P450 BM3 mutants able to hydroxylate linear alkanes (94). However, a comparison of the sensitivity of Purpald and MBTH for various aldehydes showed that MBTH is 5X more responsive to propanal, butanal, and pentanal (95), which are of similar chain lengths to our target alcohols. Therefore, we decided to develop an assay for 3-methyl-3-butenol, 3-methyl-2-butenol, and 3-methyl-butanol using MBTH.

Materials and Methods

Culture conditions. *E. coli* harboring one of various Nudix hydrolase genes and the mevalonate pathway genes as described in Chapter 2 were grown overnight at 37°C in either 5 mL in culture tubes or 500 µL in 96-well plates in Luria Broth medium. The overnight cultures were inoculated into fresh EZ Rich Defined Medium (Teknova) containing 0.5 mM isopropyl β-D-1-thiogalactopyranoside (IPTG) (Sigma-Aldrich) and grown at 30°C for 18-20 hrs. The cultures were centrifuged, and the supernatant was assayed using MBTH.

GC analysis. 3-methyl-3-butenol production was verified using GC as described in Chapter 2.

MBTH assay. The standard reaction mixture for the MBTH assay contained the following in 200 µL: 8µL of a MBTH solution, 40 µL of an acid solution, 10 µL of sample, and 142 µL of H_2O. The MBTH (Sigma-Aldrich) solution is made by dissolving MBTH in H_2O to a final concentration of 3 mg/mL. The acid solution is made by dissolving 0.5 g of ferric ammonium sulfate (Sigma-Aldrich) and 0.5 g of sulfamic acid (Sigma-Aldrich) in 100 mL H_2O (96). To analyze a sample, the MBTH solution, sample, and H_2O are mixed together first for 15 min at room temperature. Afterwards, the acid solution is added to the mixture, which is incubated at room temperature for 30 min before reading its absorbance at 620 nm using a Spectramax M2 (Molecular Devices). 3-methyl-3-butenol, 3-methyl-2-butenol, 3-methyl-butanol, butanol, and ethanol standards were purchased from Sigma-Aldrich and used to determine the linear range of the assay for each alcohol. Alcohol oxidase from Pichia pastoris and Tris were purchased from-Sigma Aldrich.

Results

MBTH assay development. MBTH is commonly used to detect methanol. Methanol is first oxidized using an oxidizing agent or alcohol oxidase and converted into formaldehyde. Formaldehyde reacts with MBTH to form a blue color. The typical components of the assay are MBTH, acidic iron solution, alcohol oxidase, Tris-HCL buffer, and sample (96). We tested whether each of the five components were necessary to form a color change using a 3-methyl-3-butenol standard. We were surprised to discover that neither the alcohol oxidase nor Tris-HCl were necessary to observe the formation of the blue color (Table 1). The alcohol oxidase and Tris-HCl were also not necessary to detect 3-methyl-2-butenol and 3-methyl-butanol standards using MBTH (Fig. 6).

Table 1. Determination of the necessity of each of the five components in the MBTH assay to detect 3-methyl-3-butenol. Each of the five component was left out of the assay to determine its necessity in the formation of the blue color.

Component							
MBTH	X	X		X	X	X	X
Acidic Iron Solution	X	X	X		X	X	X
Alcohol Oxidase	X	X	X	X		X	
Tris-HCl	X	X	X	X	X		
3-methyl-3-butenol	X		X	X	X	X	X
Blue Color?	**Yes**	**No**	**No**	**No**	**Yes**	**Yes**	**Yes**

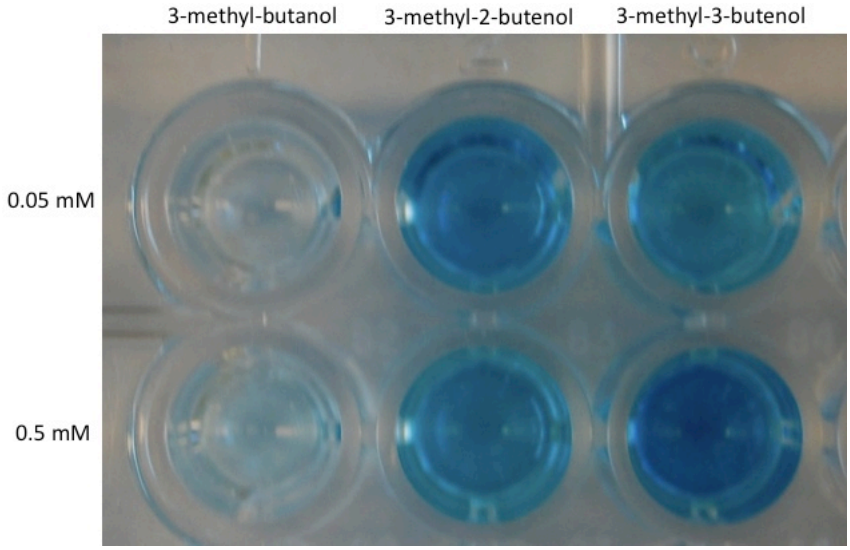

Fig. 6. The MBTH assay can detect 3-methyl-butanol, 3-methyl-2-butenol, and 3-methyl-3-butenol standards. The formation of a blue dye is observed when MBTH reacts with each alcohol, and the intensity of the color change is different for each alcohol. The color change is more intense for 3-methyl-2-butenol and 3-methyl-3-butenol than for 3-methyl-butanol.

MBTH assay is sensitive towards the five-carbon alcohol standards. The color change observed in the MBTH assay can be quantified by measuring the absorbance of the sample at 620 nm. We compared the sensitivity of the assay for 3-methyl-3-butenol, 3-methyl-2-butenol, and 3-methyl-butanol. Based on the concentrations tested, the linear range of the assay is 0.1-30 μM for 3-methyl-3-butenol, 0.1-20 μM for 3-methyl-2-butenol, and 0.1-50 mM for 3-methyl-butanol (Fig. 7). The linear range of detection for 3-methyl-2-butenol is slightly narrower with a steeper slope compared to that for 3-methyl-3-butenol, indicating that the assay is most sensitive for 3-methyl-2-butenol. Butanol was also tested to determine the selectivity of the assay, since the length of the carbon backbone of butanol is the same as the five carbon alcohols tested. No color change was observed when butanol was added as the substrate in the MBTH assay, which indicates that the assay is selective in the alcohols it reacts with as substrates.

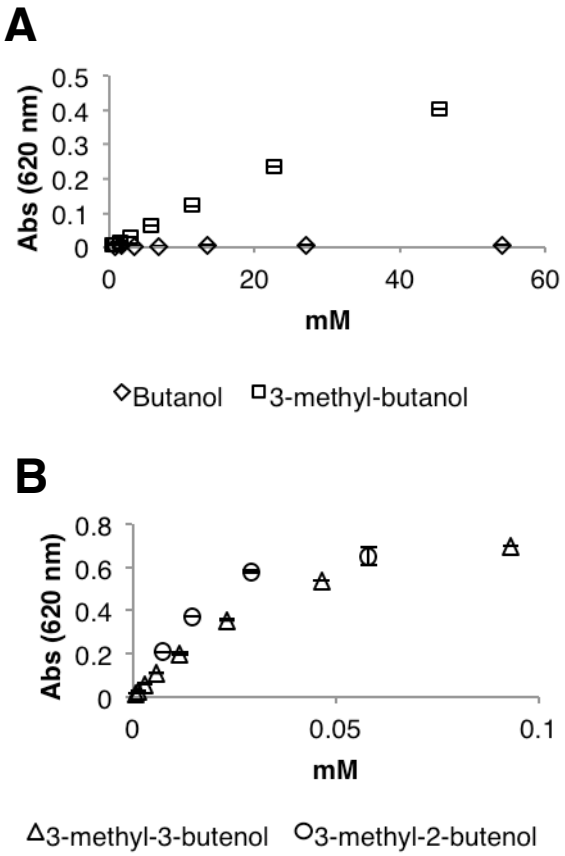

Fig. 7. MBTH assay can quantify five-carbon alcohol standards. (**A**) The MBTH assay did not detect butanol at any of the concentrations tested. The MBTH assay detected 3-methyl-butanol at all concentrations tested from 0.1-50 mM, and the change in concentration resulted in a linear change in absorbance measured at 620 nm. (**B**) The MBTH assay is more sensitive for both 3-methyl-3-butenol and 3-methyl-2-butenol compared to 3-methyl-butanol with linear ranges in the μM concentrations.

MBTH assay is sensitive for 3-methyl-3-butenol produced in cultures. Next, we tested if MBTH could detect 3-methyl-3-butenol produced from cell cultures in order to determine whether the amount of alcohol produced is within the sensitivity range of the assay, and whether components in the culture might interfere with the detection of the target alcohols. NudB was overexpressed in *Escherichia coli* harboring pMevT and pMevB to create a strain capable of producing 3-methyl-3-butenol as described in Chapter 2. A blue color was observed when the supernatant from a 24 hr culture overexpressing NudB was reacted with MBTH (Fig. 8). A less intense blue color was observed when the supernatant was from a culture overexpressing the backbone vector without NudB, which is known to produce less 3-methyl-3-butenol. A pale green color is observed when the assay was reacted with *E. coli* culture not producing any 3-methyl-3-butenol. The pale green color suggests that something in the culture reacts with some component of the assay.

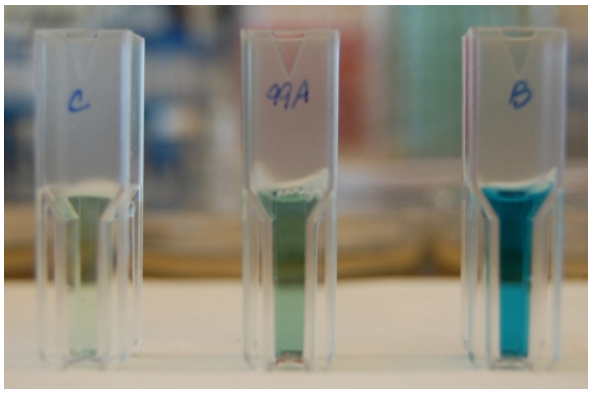

Fig. 8. MBTH assay detects 3-methyl-3-butenol produced by cell cultures. A blue color forms when MBTH is reacted with the supernatant from a culture producing 3-methyl-3-butenol (B). A less intense blue color is observed when MBTH is reacted with the supernatant from a culture producing less 3-methyl-3-butenol (99A). A pale green color is observed when MBTH is reacted with the supernatant from a culture not producing any 3-methyl-3-butenol (C).

The MBTH assay was also tested on 3-methyl-3-butenol produced by genetically modified *E. coli* overexpressing various Nudix hydrolase genes that lead to the production of different concentrations of 3-methyl-3-butenol. We determined that a minimum of 20 minutes following the addition of the acidic iron solution is necessary to differentiate between the different concentrations of 3-methyl-3-butenol produced *in vivo* (Fig. 9).

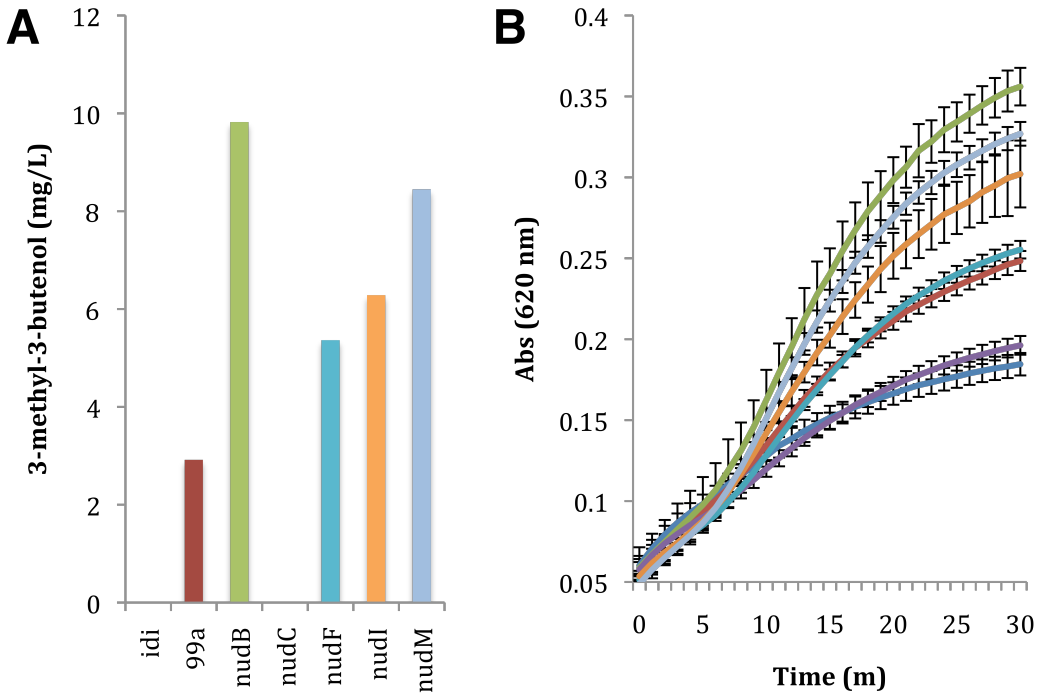

Fig. 9. MBTH assay can differentiate between different alcohol concentrations in 20 minutes. (**A**) Seven different plasmids were constructed that overexpress various genes leading to the production of different amounts of 3-methyl-3-butenol when expressed in *E. coli* harboring pMevT and pMevB. The plasmid backbone is pTrc99A (99a). idi, nudB, nudC, nudF, nudI, and

nudM indicate the gene that is overexpressed. (**B**) The supernatant from each of the cultures containing a different concentration of 3-methyl-3-butenol was reacted with MBTH. Following treatment with the acid solution, absorbance at 620 nm was measured every minute for a total of thirty minutes for each sample.

The absorbance values measured at 620 nm were compared to the production titer of 3-methyl-3-butenol quantified using gas-chromatography mass spectrometry for each sample (Fig. 10A). A linear correlation (R^2=0.97) was observed between the production titer and absorbance value. The experiment was repeated by growing the cells and performing the MBTH assay in 96-well plates (Fig. 10B). Again, a linear correlation (R^2=0.94) was observed between the production titer and absorbance value, indicating that the method is suitable for use in a 96-well format and could be developed into a high-throughput assay.

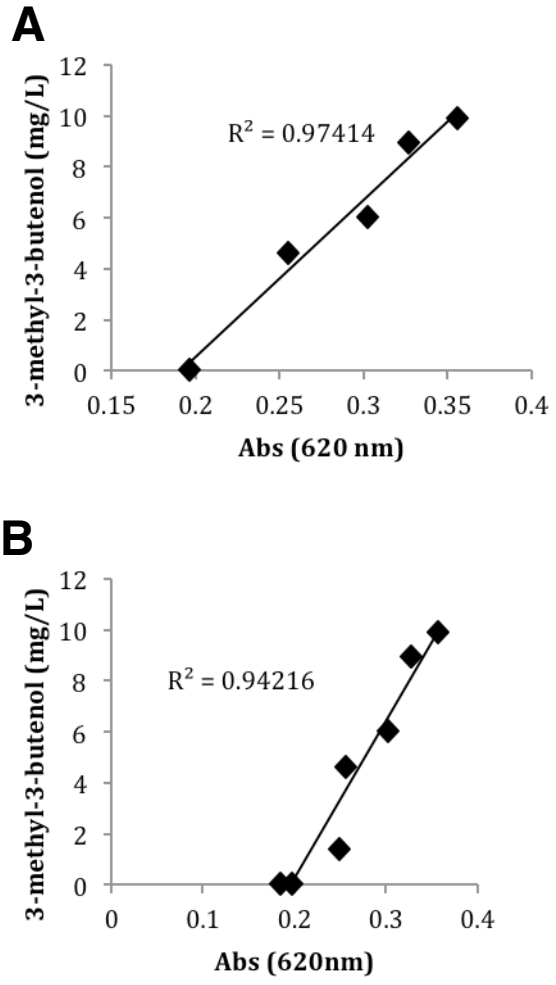

Fig. 10. MBTH assay can quantify 3-methyl-3-butenol produced in cultures. (**A**) Production titer plotted against absorbance measured at 620 nm for 3-methyl-3-butenol production by *E. coli* grown in 5 mL cultures. (**B**) Production titer plotted against absorbance measured at 620 nm for 3-methyl-3-butenol production by *E. coli* grown and assayed in 96-well plates.

Discussion

We have developed a new colorimetric assay to detect 3-methyl-3-butenol, 3-methyl-2-butenol, and 3-methyl-butanol that uses the chromogenic agent MBTH. The assay is performed at room temperature and can differentiate between different concentrations of alcohol present in 20 minutes. The color change can be detected visually and quantified by measuring the absorbance of the sample at 620 nm. The linear range of the assay is 0.1-30 μM for 3-methyl-3-butenol, 0.1-20 μM for 3-methyl-2-butenol, and 0.1-50 mM for 3-methyl-butanol. The assay is 1000X more sensitive for 3-methyl-3-butenol and 3-methyl-2-butenol than 3-methyl-butanol.

We hypothesize that the difference in sensitivity is caused by a difference in the stability of one or more intermediates formed during the assay. MBTH reacts with aldehydes to form a blue colored dye. An acidic iron solution is added to the sample in order to create an oxidizing condition that catalyzes the oxidation of the alcohol group to an aldehyde and the subsequent oxidation reactions required for the dye to form (Fig. 11). Both 3-methyl-3-butenol and 3-methyl-2-butenol have a double bond either alpha-beta or beta-gamma to the carbon with the functional group. The double bond allows resonance structures to form that might stabilize the formation of either the aldehyde intermediate or precursor to the dye. Similarly, the double bond permits a conjugated system to form that might facilitate the formation of the dye and stabilize the final product.

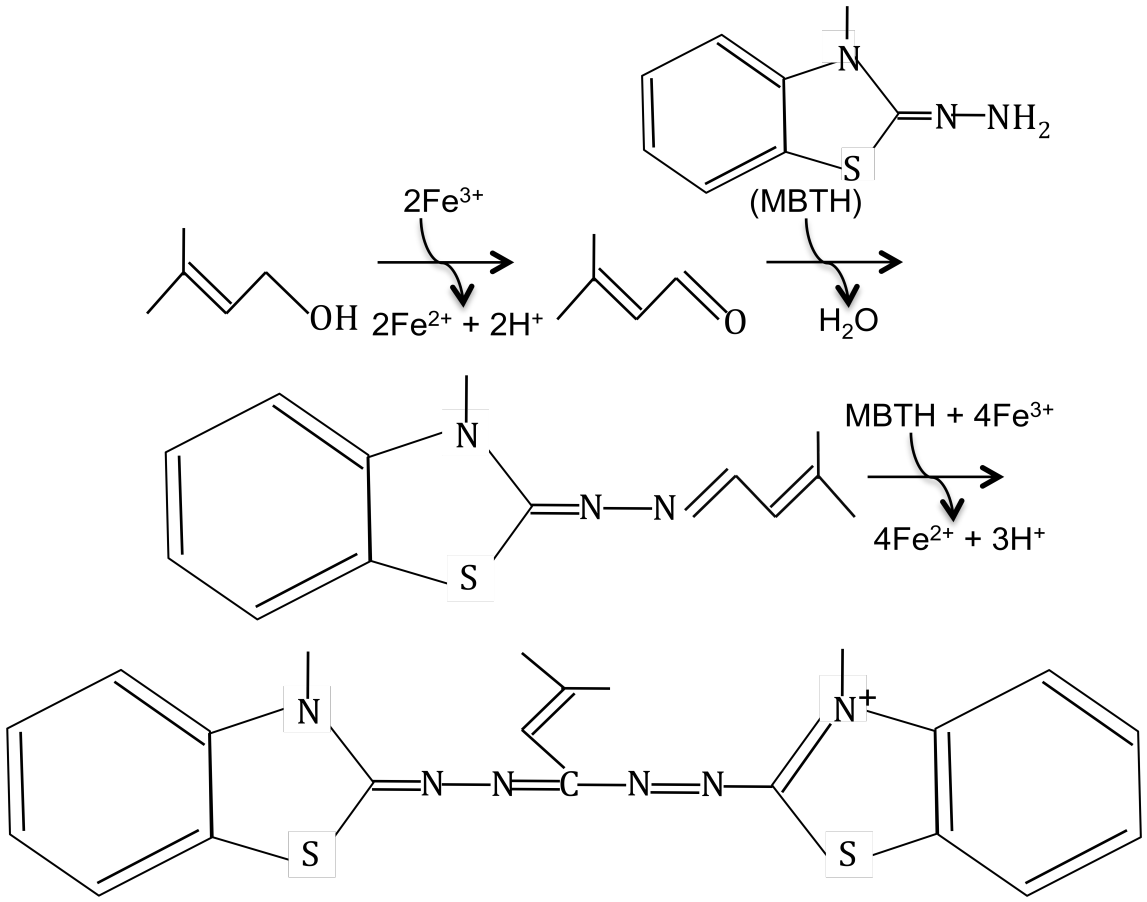

Fig. 11. 3-methyl-2-butenol reacts with MBTH to form a blue dye. Under oxidizing conditions, 3-methyl-2-butenol is oxidized into 3-methyl-2-butenal that reacts with two molecules of MBTH to form a blue colored dye. Fe^{3+} from the acidic iron solution added to the assay acts as the oxidant to catalyze the oxidation reactions.

The MBTH assay we developed did not react with butanol. However, a pale green color was observed when the supernatant from a culture that did not produce 3-methyl-3-butenol was used as the sample in the assay. The pale green color could be measured at 620 nm. The color change in the absence of 3-methyl-3-butenol production indicates that *E. coli* excretes some molecules into the media that react with MBTH. Typical fermentation byproducts from *E. coli* are short-chain acids and alcohols, such as formate, acetate, lactate, and ethanol. It is unlikely that the short-chain acids are the cause of the pale green color, because MBTH reacts with aldehydes and the acids would not be converted into aldehydes in the oxidizing conditions of the assay. It is also unlikely that ethanol is the source of the pale green color, because, like butanol, no color change was observed when an ethanol standard purchased from Sigma-Aldrich was used in the assay (data not shown).

Despite the pale green color observed from samples not producing 3-methyl-3-butenol, a significant color change was observed in the presence of 3-methyl-3-butenol produced *in vivo*, and the intensity of the color change correlated with the different concentrations of 3-methyl-3-butenol (R^2=0.97). Furthermore, a strong correlation between production and color change was also observed when the cultures were grown in 96 well plates (R^2=0.94). Therefore, for the purpose of detecting 3-methyl-3-butenol, 3-methyl-2-butenol, and 3-methyl-butanol in a high-throughput assay to engineer increased production in *E. coli*, the MBTH assay we have developed is sufficient. The transition from a GC based assay to the MBTH assay will increase the throughput for analyzing mutants to 10^4 samples/instrument/day. This throughput is sufficient for the analysis of mutants generated using existing rational and random mutagenesis techniques.

Chapter 4: Programming Adaptive Control to Evolve Increased Isopentenyl Diphosphate Production

Abstract

The complexity inherent in biological systems challenges efforts to rationally engineer novel phenotypes, especially those not amenable to high-throughput screens and selections. In nature, adaptation can rapidly evolve new traits by changing the mutation rate in a cell. Based on theory and experimental data, we constructed an adaptive control process that mimics natural adaptation by programming cells to change their mutation rate based on a particular desired phenotype. This system is called feedback-regulated evolution of phenotype (FREP), and is implemented with a sensor to gauge the target phenotype and an actuator to alter the mutation rate. To evolve certain novel traits that have no known natural sensors, we developed a framework to assemble synthetic transcription factors and used it to construct four different sensors that recognize isopentenyl diphosphate in bacteria and yeast. We verified FREP by evolving increased tyrosine and isoprenoid production. Taken together, our work demonstrates how complex behaviors could be rationally engineered using control-based systems.

Introduction

Adaptation is a behavior that allows cells to survive and thrive in constantly changing environmental conditions and is characterized by rapid genetic change creating rare beneficial mutations (55). The appearance of microbial strains with higher than average mutation rates accompany periods of adaptation in both natural and laboratory environments (56, 57, 58). Models and experimental data of the adaptive process indicate a variable mutation rate strategy is used to evolve traits, where increased mutation rates are only beneficial to populations with low phenotypic diversity, while populations with high degrees of diversity benefit from decreased mutation rates (59, 60, 61).

Many mutagenesis strategies to generate diversity in the laboratory exist, but most industrially important phenotypes are not amenable to the high-throughput screens and selections required to isolate mutants exhibiting the desired traits (62, 63). Furthermore, directed evolution strategies that generate mutant libraries *in vitro* are limited by the transformation efficiency of the cell, and those that use mutator strains with unregulated, high mutation rates to generate mutant libraries *in vivo* (64) suffer from the accumulation of deleterious mutations that eventually lead to cell death. Although adaptation has proven useful for evolving certain phenotypes, its application is limited to traits that are directly tied to growth (65). Therefore, a method capable of regulating mutagenesis *in vivo* according to a particular phenotype, independent of whether it is linked to growth, could circumvent the constraints set by transformation inefficiencies, deleterious mutations, and assay availability.

We created such a method by implementing the variable mutation rate strategy to evolve new traits using an adaptive control system (66) we call feedback-regulated evolution of phenotype (FREP) (Fig. 12A). FREP consists of two modules that control the mutation rate of the genome (M) based on the concentration of a ligand (L) associated with the target phenotype being evolved. The actuator module converts a transcriptional signal (T) into M, and the sensor module modifies T by converting L into a change in transcriptional signal (ΔT). M affects L over time as beneficial mutations for the target phenotype are generated in the genome, creating a feedback loop that causes M to decrease as L increases. The sensor is assembled from two components: a transcription factor (TF) that binds the target ligand and a promoter regulated by the TF. Depending on the target ligand, FREP could evolve a phenotype at either the population or single-cell level (Fig. 12B). If the ligand is diffusible across the cell membrane and the rate of diffusion >> dL/dt, then the effect of FREP is averaged across the entire population. However, if the ligand is not diffusible across the cell membrane or its diffusion across the membrane is << dL/dt, then FREP acts on each individual cell separately. Here we demonstrate the application of FREP to each ligand type.

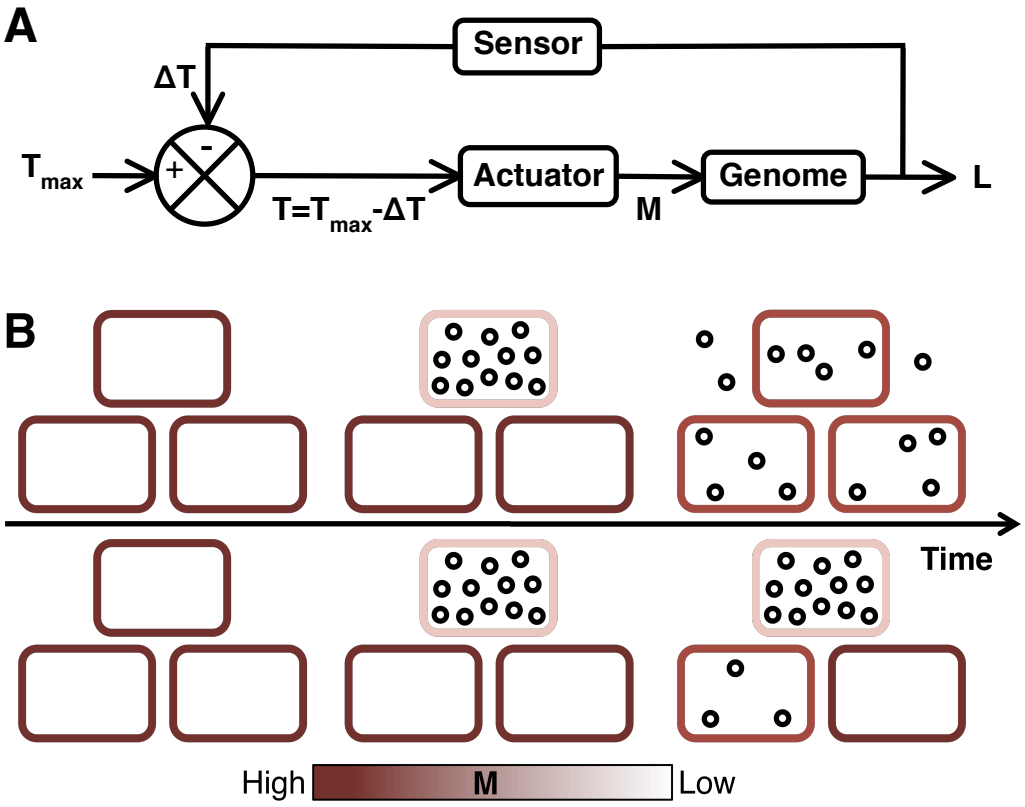

Fig. 12. FREP design. **(A)** FREP implementation of the variable mutation strategy using an adaptive control system. The sensor controls the change in transcriptional level (ΔT) in the system. The actuator converts the transcriptional level (T) into a mutation rate (M) that modifies the genome to produce the target phenotype gauged by L. As L increases, the sensor increases ΔT, which causes the actuator to decrease M. **(B)** Two different outcomes of FREP are possible depending on whether the ligand is permeable to the cell membrane. Circles represent the

concentration of ligand in the cell. If the ligand is permeable to the membrane, then a few or a single, high-level producer of L could reduce M in all other cells, causing the entire population to stop evolving independent of each cell's level of L (top). If the ligand is not permeable to the membrane, then each cell in the population evolves independently of the other cells (bottom).

Materials and Methods

Oligonucleotides and DNA sequencing. All oligonucleotides were obtained from Integrated DNA Technologies with standard purification. Primer sequences mentioned here are presented in Appendix A.2. DNA sequencing to confirm cloning products was performed by Quintara Biosciences.

Strains and plasmids availability. Strains, plasmids, and plasmid sequences (in Genbank format) constructed in this study are deposited in the private instance of the JBEI registry and will be moved to the public instance (https://public-registry.jbei.org) after publication. Strains and plasmids are physically available from Addgene (http://www.addgene.org).

Strains. We cloned the kanamycin cassette from pKD4 into pMevB (9) to contruct pMevB-Kan using the primers Kan-F and Kan-R. We engineered EcHC175 by amplifying *mk*, *pmk*, and *pmd* of the mevalonate operon with the kanamycine cassette from pMevB-Kan with the primers IdiKO-F and IdiKO-R (homology sequences shown in italics in Appendix A.2) and knocking out *idi* in *E. coli* MG1655 with the PCR product according to Datsenko & Wanner (84). *E. coli* DJ106, DJ166, and DJ238 were gifts from Dr. Darmawi Juminaga. *S. cerevisiae* MO219 was a gift from Dr. Mario Ouellet. All genes and promoter sequences amplified from the *E. coli* chromosome were from MG1655. All genes amplified from the *S. cerevisiae* chromosome were from BY4742.

Construction of pLyc. We cloned *crtE*, *crtI*, and *crtB* from pT-LYCm4 (gift from Dr. Adrienne McKee) into pBAD18-Cm using the restriction enzymes SpeI and HindIII following standard restriction digest and ligation cloning protocols.

Construction of plasmids containing E. coli IPP sensor modules. pCtl-RFP-S_{AraC} (S_{AraC}: sensor module containing the transcription factor (TF) AraC) was constructed by removing HindIII from pBAD24 using QuickChange PCR with the primers DelHindIII-F and DelHindIII-R (where HindIII was removed is underlined in Appendix A.2), cloning the DNA sequence from araC to P_{BAD} from pBAD24M-gfp (6) using ClaI and EcoRI, and cloning *mutD* amplified from *E. coli* using the primers MutD-F and MutD-R and *mcherry* using the primers RFP-F and RFP-R 3' of the *araBAD* promoter, P_{BAD}.

The chimeric protein IA was constructed by fusing *idi* to the C-terminus of *araC* using SOEing PCR. *idi* was amplified from *E. coli* using the primers Idi-F and Idi-SOE-R, and the linker and C-terminus of *araC* were amplified from pBAD24 using the primers AraC-SOE-F and AraC-R. These two PCR products were templates for SOEing PCR using Idi-F and AraC-R to amplify the chimeric protein. We cloned IA into pCtl-RFP-S_{AraC} by

replacing AraC to make pCtl-RFP-S_{IA} (S_{IA}: sensor module containing the synthetic TF IA).

Mutants of IA were generated using the GeneMorph II Random Mutagenesis Kit (Agilent Technologies) according to the manufacturer's instructions. We cloned the IA mutants into pCtl-RFP-S_{IA} using Idi-F and AraC-R, transformed the constructs into EcHC175, and screened for changes in RFP expression relative to IA in the presence (10 mM) and absence (0 mM) of mevalonate induced with 0.1 mM isopropyl β-D-1-thiogalactopyranoside (IPTG) (Sigma-Aldrich). RFP was measured using a Spectramax M2 (Molecular Devices) exciting at 587 nm and measuring emission at 610 nm. We isolated two mutants of interest: IA32 and IA44. pCtl-RFP-S_{AC} were constructed by amplifying the C-terminal domain of AraC with the primers AC-F and AraC-R, and cloning into pCtl-RFP-S_{AraC}. pCtl-RFP-S_{IA44} was digested with ClaI and KpnI, and the fragment containing IA44 to mutD was cloned into pBAD24 to construct pCtl-S_{IA44}.

Construction of plasmids containing mutD5 mutator module. The mutator *mutD5* was a gift from Dr. Adrienne McKee and cloned into pCtl-S_{IA44}, pCtl-RFP-S_{AraC}, pCtl-RFP-S_{IA44}, and pCtl-RFP-S_{aroF3} using the primers MutD-F and MutD-R to replace *mutD* and make pMut-S_{IA44}, pMut-RFP-S_{AraC}, pMut-RFP-S_{IA44}, and pMut-RFP-S_{aroF3}. pMut-S_{AC}, pMut-S_{AraC}, pMut-S_{IA32} were constructed by cutting the TF from pCtl-RFP-S_{AC}, pCtl-RFP-S_{AraC}, pCtl-RFP-S_{IA32} using ClaI and HindIII, and cloning the fragments into pMut-S_{IA44}.

Characterization of E. coli IPP sensor modules. We measured expression of RFP from P_{BAD} controlled by one of the TFs (AraC, AC, IA, IA32, or IA44) by transforming pCtl-RFP-S (S designates a sensor module with one of the TFs) into EcHC175 and plating on LB agar plates with ampicillin and kanamycin. We picked three clones from each plate, grew each clone in LB medium with antibiotics overnight, and inoculated each culture into fresh EZ Rich Defined Medium (Teknova) with antibiotics to an initial Abs_{600} of 0.05 the following day. Each fresh culture was grown for 3 hours at 37°C, induced with IPTG (0.1 mM) and mevalonate (0-10 mM) (or 0-10 mM arabinose for AraC), and grown for an additional 17 hours at 37°C. We measured RFP fluorescence using a Spectramax M2 (Molecular Devices) exciting at 495 nm and measuring emission at 520 nm. Abs_{600} was also measured using a Spectramax M2.

To determine IA's binding sequence upstream of P_{BAD}, we amplified I_1I_1 using the primer I1I1-F, I_2I_1 using the primer I2I1-F, or I_2I_2 using the primer I2I2-F, all paired with AraReg-R and using pCtl-RFP-S_{IA} as template. The PCR products were cloned into pCtl-RFP-S_{IA} to replace the I_1I_2 sequence to make pCtl-RFP-S_{IA}-I_1I_1, pCtl-RFP-S_{IA}-I_2I_1, and pCtl-RFP-S_{IA}-I_2I_1. RFP expression from the modified binding sequences was determined as described above.

We amplified CFP using the primers CFP-F and CFP-R, and inserted it 3' of the TF expressed 3' of P_c into pCtl-RFP-S_{AC}, pCtl-RFP-S_{AraC}, and pCtl-RFP-S_{IA} to make pCtl-CFP-RFP-S_{AC}, pCtl-CFP-RFP-S_{AraC}, and pCtl-CFP-RFP-S_{IA}. RFP and CFP expression from these constructs were determined as indicated above, and CFP fluorescence was

measured using a Spectramax M2 (Molecular Devices) exciting at 433 nm and measuring emission at 475 nm.

Construction of plasmids containing tyrosine sensor modules. We replaced P_C with CP20 (85) in pCtl-RFP-S_{AraC} using the primers CP20-F and CP20-R, and cloned in *tyrR* amplified from *E. coli* using the primers TyrR-F and TyrR-R to construct pCtl-RFP-TyrR.

pCtl-RFP-S_{aroF0} was constructed by amplifying the promoter region of *aroF* from *E. coli* using the primers AroF0-F and AroF0-R, and cloning the PCR product into pCtl-RFP-TyrR to replace P_{BAD}. pCtl-RFP-S_{aroF1} was constructed by mutating TyrR with the primers TyrR-E274Q-F and TyrR-E274Q-R to make TyrR E274Q (86), and cloning the PCR product into pCtl-RFP-S_{aroF0}. pCtl-RFP-S_{aroF2} was constructed by mutating TyrR with the primers TyrR-N316K-F and TyrR-N316K-R to make TyrR N316K (87), and cloning the PCR product into pCtl-RFP-S_{aroF0}. pCtl-RFP-S_{aroF3} was constructed by mutating TyrR E274Q with the primers TyrR-N316K-F and TyrR-N316K-R, and cloning the PCR product into pCtl-RFP-S_{aroF0}. The N-terminus of TyrR was also truncated to different lengths to generate TyrR Δ43, TyrR Δ93, and TyrR Δ187 (88). pCtl-RFP-S_{aroF4} was constructed by amplifying TyrR with the primers Del43TyrR-F and TyrR-R, and cloning the PCR product into pCtl-RFP-S_{aroF0}. pCtl-RFP-S_{aroF5} was constructed by amplifying TyrR with the primers Del93TyrR-F and TyrR-R, and cloning the PCR product into pCtl-RFP-S_{aroF0}. pCtl-RFP-S_{aroF6} was constructed by amplifying TyrR with the primers Del187TyrR-F and TyrR-R, and cloning the PCR product into pCtl-RFP-S_{aroF0}.

pCtl-RFP-S_{aroL0} was constructed by replacing P_{BAD} with the promoter region of *aroL* from *E. coli* using the primers AroL0-F and AroL0-R, and cloning the PCR product into pCtl-RFP-TyrR. TyrR from pCtl-RFP-S_{aroF1}, pCtl-RFP-S_{aroF2}, and pCtl-RFP-S_{aroF3} were amplified using the primers TyrR-F and TyrR-R and cloned into pCtl-RFP-S_{aroL0} to construct pCtl-RFP-S_{aroL1}, pCtl-RFP-S_{aroL2}, and pCtl-RFP-S_{aroL3}, respectively. The TyrR boxes 1, 2, 3 of the promoter P_{aroL} were also modified to tune TyrR regulation of the promoter (89). pCtl-RFP-S_{aroL4} was constructed by modifying the sequences of box 1 and 2 of P_{aroL} in pCtl-RFP-S_{aroL0} with the primers AroLBox1and2-F and AroLBox1and2-R. pCtl-RFP-S_{aroL5} was constructed by modifying the box 3 sequence of P_{aroL} in pCtl-RFP-S_{aroL0} with the primers AroLBox3-F and AroLBox3-R.

pCtl-RFP-S_{aroP0} was constructed by replacing P_{BAD} with the promoter region of *aroP* from *E. coli* using the primers AroP0-F and AroP0-R, and cloning the PCR product into pCtl-RFP-TyrR. TyrR from pCtl-RFP-S_{aroF1}, pCtl-RFP-S_{aroF2}, and pCtl-RFP-S_{aroF3} were amplified using the primers TyrR-F and TyrR-R and cloned into pCtl-RFP-S_{aroP0} to construct pCtl-RFP-S_{aroP1}, pCtl-RFP-S_{aroP2}, and pCtl-RFP-S_{aroP3}, respectively. pCtl-RFP-S_{aroP4} was constructed by modifying the P_2 sequence of P_{aroP} to make P_{2up} (90) in pCtl-RFP-S_{aroP0} with the primers P2UP-F and P2UP-R. pCtl-RFP-S_{aroP5} and pCtl-RFP-S_{aroP6} were constructed by amplifying TyrRΔ43 and TyrRΔ93 from pCtl-RFP-S_{aroF4} and pCtl-RFP-S_{aroF5}, respectively, using the primers Del43TyrR-F or Del93TyrR-F paired with TyrR-R, and cloning the PCR products into pCtl-RFP-S_{aroP4}.

Characterization of tyrosine sensor modules. Plasmids containing each of the twenty tyrosine sensor modules described above were transformed into *E. coli* DJ106 and DJ166, and plated on LB agar with ampicillin. Clones were grown overnight in LB medium with ampicillin, inoculated into EZ Rich Defined Medium the next day to an initial Abs_{600} of 0.05, and tyrosine production was quantified after 20 hours. RFP fluorescence and Abs_{600} were measured as described earlier. The experiment was repeated in triplicate for S_{aroF3}, S_{aroL5}, and S_{aroP6}.

Construction of yeast synthetic transcription factors and IPP sensor modules. The TEF promoter was amplified and cloned into pESC-Ura to make pESC-P_{TEF} using the primers TEF-F and TEF-R. yEcitrine was amplified and cloned into pESC-P_{TEF} behind P_{gal10} to make pESC-YFP-P_{TEF} using the primers YEcitrine-F and YEcitrine-R. The cyc1 terminator and TEF promoter were fused using SOEing PCR with the primers CYC1-SOE-F, CYC1-SOE-R, TEF-SOE-F, and TEF-SOE-R to make the PCR product P_{TEF2}.

idi was fused to the activator and DNA-binding domains of *gal4*, respectively, using SOEing PCR with *idi* being 3' of the *gal4* domains. The activator domain of *gal4* was amplified from *S. cerevisiae* using the primers AD-F and AD-SOE-R. The DNA binding domain of *gal4* was amplified from *S. cerevisiae* using the following primers: DBD-F and DBD-SOE-R. The AD-SOE-R and DBD-SOE-R primers included the linker sequence joining the domains to *idi*. *idi* was amplified from *E. coli* using the primers GI-SOE-F with AD-GI-R or GI-SOE-F with DBD-GI-R. The PCR product of AD-F and AD-SOE-R was fused to the product of GI-SOE-F and AD-GI-R to make AD-GI. The PCR product of DBD-F and DBD-SOE-R was fused to the product of GI-SOE-F and DBD-GI-R to make DBD-GI. AD-GI, P_{TEF2}, and DBD-GI were cloned into pESC-YFP-P_{TEF} behind P_{TEF} to make pESC-YFP-$S_{Idi\text{-}GAL4}$.

idi1 was fused to the activator and DNA binding domains of *gal4*, respectively, using SOEing PCR with *idi1* being 3' of the *gal4* domains. *Idi1* was amplified from *S. cerevisiae* using the primers GI1-SOE-F and AD-GI1-R or GI1-SOE-F and DBD-GI1-R. The PCR product of AD-F and AD-SOE-R was fused to the product of GI1-SOE-F and AD-GI1-R to make AD-GI1. The PCR product of DBD-F and DBD-SOE-R was fused to the product of GI1-SOE-F and DBD-GI1-R to make DBD-GI1. AD-GI1, P_{TEF2}, and DBD-GI1 were cloned into pESC-YFP-P_{TEF} behind P_{TEF} to make pESC-YFP-$S_{Idi1\text{-}GAL4}$.

erg20 was fused to the activator and DNA binding domains of *gal4*, respectively, using SOEing PCR with *erg20* being 3' of the *gal4* domains. *erg20* was amplified from *S. cerevisiae* using the primers GE20-SOE-F with AD-GE20-R or GE20-SOE-F with DBD-GE20-R. HindIII and KpnI were removed from *erg20* using the primers DelHindIII-Erg20-F, DelHindIII-Erg20-R, DelKpnI-Erg20-F, and DelKpnI-Erg20-R (where HindIII and KpnI were removed are underlined). The PCR product of AD-F and AD-SOE-R was fused to the product of GE20-SOE-F and AD-GE20-R to make AD-GE20. The PCR product of DBD-F and DBD-SOE-R was fused to the product of GE20-SOE-F and DBD-GE20-R to make DBD-GE20. AD-GE20, P_{TEF2}, and DBD-GE20 were cloned into pESC-YFP-P_{TEF} 3' of P_{TEF} to make pESC-YFP-$S_{Erg20\text{-}GAL4}$.

Characterization of yeast IPP sensor modules. pESC-YFP-P_{TEF}, pESC-YFP-$S_{Idi\text{-}GAL4}$, pESC-YFP-$S_{Idi1\text{-}GAL4}$, and pESC-YFP-$S_{Erg20\text{-}GAL4}$ were transformed into ScMO219 using electroporation, plated on Synthetic Defined (SD) agar without uracil and with 2% glucose, and grown at 30°C for 3 days. SD medium was composed of 1X CSM without the appropriate amino acids (Sunrise Science Products) and 1X Difco Yeast Nitrogen Base without amino acids (BD), prepared according to the manufacturers' instructions. Three clones from each plate were grown overnight in SD medium without uracil and with 2% glucose, inoculated into fresh medium without uracil and with 1.8% galactose and 0.2% glucose the following day to an initial Abs_{600} of 0.05, and grown for 3 days at 30°C. YFP fluorescence was measured using a Spectramax M2 (Molecular Devices) exciting at 516 nm and measuring emission at 529 nm, and normalized to OD measured at 600 nm.

Protein purification of IA. We amplified IA tagged with Strep-tag II on the C-terminus using the primers IA-StrepII-F and IA-StrepII-R (Strep-tag II sequence is in italics), and cloned the PCR product into pPro29b (32) after the promoter P_{prpB} to make pPro29b-IA. BLR(DE3) *E. coli* was transformed with pPro29b-IA, and an overnight culture was inoculated into a liter of LB medium with ampicillin to an initial Abs_{600} of 0.05. We grew the culture at 37°C until the Abs_{600} reached 0.6, induced it with 20 mM propionate, and grew it overnight at 20°C. The cells were pelleted, resuspended in binding buffer (20 mM sodium phosphate, 280 nM NaCl, 6 mM potassium chloride, pH 7.4), sonicated, and centrifuged. The tagged protein was purified from the supernatant with a gravity flow column using StrepTactin Sepharose High Performance (GE Healthcare) following the manufacturer's instructions. Protein concentration was determined using the Pierce BCA Protein Assay Kit (Thermo Scientific).

Gel electrophoresis mobility shift assay (EMSA). The region from the promoters P_C to P_{BAD} was amplified from pCtl-RFP-S_{AraC} using the primers EMSA-AraReg-F and EMSA-AraReg-R. I_1 of the region between P_C and P_{BAD} was synthesized using the primers EMSA-I1-F and EMSA-I1-R. I_1I_2 of the region between P_C and P_{BAD} was synthesized using the primers EMSA-I1I2-F and EMSA-I1I2-R**.** Cy5 indicates that the primer was labeled with the Cy5 fluorophore (Appendix A.2). DNA duplexes were synthesized from the primers by mixing the pairs of oligonucleotides at 10 μM concentration in Phusion HF PCR buffer (New England BioLabs), heating for 1 min at 95°C, and cooling to 25°C over 1 hour. We incubated purified IA (0-10 nM) with Cy5 labeled DNA duplexes (20 nM) in binding buffer (10 mM Tris-HCl, 1 mM EDTA, 100 mM KCl, 1 mM dithioerythritol, 5% glycerol, pH 7.4) at room temperature (20°C ± 2°C) for 20 min. 10 μM IPP was added to test its effect on IA binding to DNA. Samples were prepared and run on a 6% DNA retardation gel (Invitrogen) according to the manufacturer's instructions. Gels were viewed using MultiImage III (Alpha Innotech) equipped with a Cy5 filter.

FRET DNA binding assay. I_1 of the region between the promoters P_C and P_{BAD} was synthesized using the primers: I1-1F, I1-2F, I1-3R, and I1-4R. FL indicates that the primer was labeled with 6-FAM fluorescein fluorophore, and BQ indicates that the

primer was labeled with Black Hole Quencher 1. Two pairs of duplexes were synthesized from the primers: I_1-FL from pairing I_1-1F and I_1-4R, and I_1-BQ from pairing I_1-2F and I1-3R. We synthesized DNA duplexes from the primers by mixing each pair of oligonucleotides at 10 μM concentration in Phusion HF PCR buffer, heating for 1 min at 95°C, and cooling to 25°C over 1 hour. A negative control duplex I_1-NC was synthesized using unlabeled I_1-3R.

IA's ability to bind I_1 was determined by incubating purified IA (0-20 nM) with I_1-FL (100 nM) and I_1-BQ (125 nM) in binding buffer (10 mM Tris-HCl, pH 7.4, 1 mM EDTA, 100 mM KCl, 1 mM dithioerythritol, 5% glycerol) at room temperature (20°C ± 2°C) for 15 min. Fluorescence measurements were made with a Spectramax M2 (Molecular Devices) exciting at 495 nm and measuring emission at 520 nm. The experiment was performed in triplicate.

We synthesized I_1I_2 DNA duplexes using the primers I1I2-1F, I1I2-2F, I1I2-3R, and I1I2-4R. An unlabeled I1I2-3R primer was used to synthesize a negative control duplex. IA's ability to bind I_1I_2 was determined as described above. IPP (500 nM) was added to test its effect on IA binding to I_1I_2. The experiment was performed in triplicate.

Luria-Delbruck fluctuation analysis. We transformed *E. coli* MG1655 with pMut-S_{IA44}, and grew different dilutions of the transformation on LB agar plates with ampicillin for 1 day at 37°C. Thirty colonies were picked and resuspended in 100 ul of water. 50 ul of each sample was plated on a LB agar plate with 100 μg/ml rifampicin, and 50 uL for six colonies was serially diluted and plated on LB agar plates. The plates were incubated overnight at 37°C. Colonies on each plate were counted using an automated colony counting software provided with the Biospectrum Multispectral Imaging System (Ultra-Violet Products Ltd.). Mutation rates were calculated using FALCOR (91) with the "MSS Maximum Likelihood Estimator" setting. The experiment was repeated with pMut-S_{AC}, pMut-S_{IA32}, pNeg-S_{IA44}.

Assessing phenotypic distribution after 24 hours of FREP. For evolving increased IPP production, we transformed *E. coli* MG1655 with pMut-RFP-S_{IA44}, and grew different dilutions of the transformation on a LB agar plate with ampicillin for 1 day at 37°C. Ten mutants with the lowest RFP expression by visual inspection were picked, inoculated into LB medium with ampicillin, and grown overnight at 37°C. Overnight cultures of each mutant were inoculated into fresh LB medium the next day to an Abs_{600} of 0.05, grown to an Abs_{600} of 0.4 at 37°C, made electrocompetent, transformed with pLyc, plated on a LB agar plate with chloramphenicol, and grown for 1 day at 37°C. We picked a colony from each plate, inoculated it into LB medium with chloramphenicol, and assayed it for lycopene production. The same experiment was repeated with pMut-RFP-S_{AraC}, except 10 mM arabinose was added to the LB agar plates and medium.

For evolution of increased tyrosine production, we transformed DJ238 with pMut-RFP-S_{aroF3}, plated on a LB agar plate with ampicillin, and grew the transformants for 1 day at 37°C. Ten mutants with the lowest RFP expression by visual inspection were picked from the plate, inoculated into MOPS minimal medium with 0.5% glucose and

ampicillin, and grown for 24 h at 37°C. Each culture was assayed for tyrosine production.

Long-term experiment for increased lycopene production using FREP. *E. coli* MG1655 were transformed with pMut-S_{IA44} and pLyc. Cells were plated on a LB agar plate with ampicillin and chloramphenicol, and grown for 2 days at 37°C. We picked ten colonies and assayed each for lycopene production. The colony that produced the most lycopene was passaged to evolve further, and the average of the three highest production levels is reported. A total of 6 passages was performed to evolve over 432 hours. The same experiment was repeated with pMut-S_{IA32} and pMut-S_{AraC}. 10 mM arabinose was added to the LB agar plates with antibiotics for pMut-S_{AraC}.

Assay for lycopene production. Cells were grown in LB medium with antibiotics for 20 hours at 37°C. We centrifuged 1 ml of culture at 13,000 × g for 1min, removed the supernatant, and washed the pellet with 1 ml of water. 1 mL of acetone was added to the washed pellet, and the sample was vortexed and incubated at 55°C for 15 min. We centrifuged the sample at 13,000 × g for 1 min, transferred the supernatant to a cuvette, and measured the absorbance at 470 nm with a spectrophotometer. The Abs_{470} data was calibrated to a lycopene standard purchased from Sigma-Aldrich. The amount of lycopene extracted from a culture was normalized to the dry cell weight (dcw) calculated from the Abs_{600} (0.41 g dcw/Abs_{600} (92)).

Assay for L-tyrosine production. Cells were grown in either LB or MOPS minimal medium with 0.5% glucose and antibiotics for 20 hours at 37°C. 500 μL of culture was centrifuged at 13,000 × g for 1min, the supernatant was filtered through a 0.452 μm centrifugal filter (VWR) and used for HPLC analysis. We measured L-tyrosine using an Agilent 1200 Series HPLC system with a photodiode array detector set at wavelengths 210, 254, and 280 nm. The samples were separated using a reverse phase C_{18} column (Inertsil 2.1 x 250 mm, 3.5 μm from GL Sciences, Inc.). The following linear gradient of water (solvent A) and methanol (solvent B) was used with a flow rate of 0.15 ml/min: 5% B from 0-8 min, 5-40% B from 8-13 min, hold at 40% B from 13-16 min, 40-5% B from 16-21 min, and equilibrate at 5% B for 10 min. L-tyrosine data were verified using LC-MS as described elsewhere (*13*). L-tyrosine concentrations were calibrated to standards purchased from Sigma-Aldrich.

Results

We performed FREP to increase production of the industrially important amino acid tyrosine (67) in *Escherichia coli* using the tyrosine-responsive TF TyrR (68) to regulate expression of the mutator *mutD5* (69) (Fig. 13).

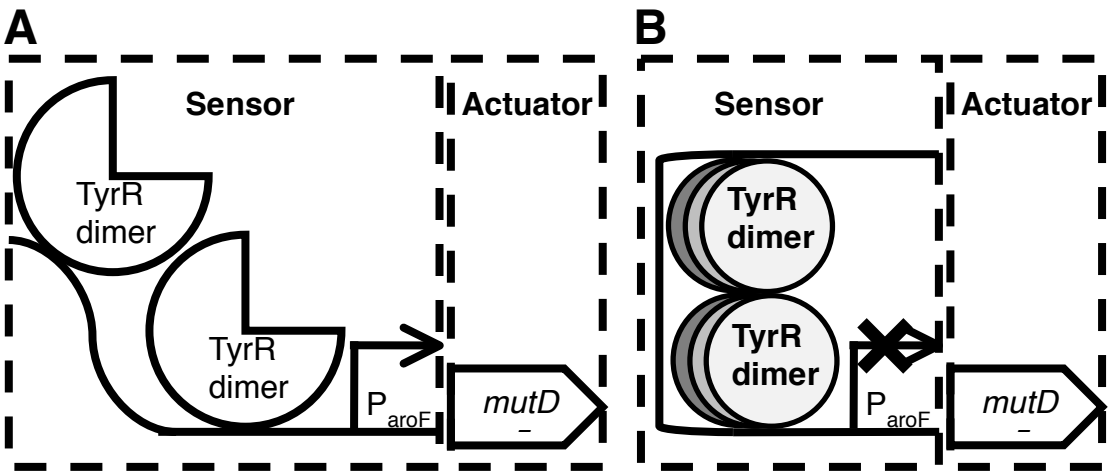

Fig. 13. FREP design to increase tyrosine production. (**A**) In one design, the sensor consists of TyrR and P_{aroF}, and the actuator consists of *mutD5*. TyrR dimers activate transcription from P_{aroF} in the absence of tyrosine. (**B**) Tyrosine-bound TyrR form hexamers that dimerize to repress transcription from P_{aroF}.

In this implementation, M should be high initially because the tyrosine concentration (L) is low, and M is reduced as beneficial mutations that increase tyrosine production appear. We modified TyrR and three TyrR-regulated promoters (P_{aroF}, P_{aroL}, P_{aroP}) to construct twenty different sensors, and screened their response to tyrosine in *E. coli* DJ106 and DJ166, two derivatives of BLR that produce different amounts of tyrosine. We monitored each sensor's output with the fluorescent protein mcherry (Figs. 14-16).

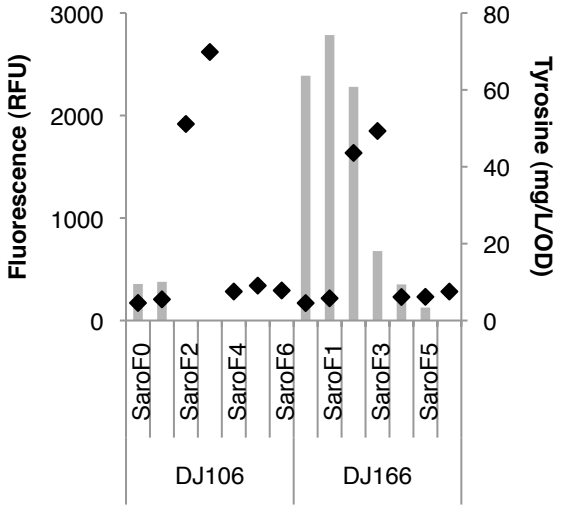

Name	TyrR Modification	P_{aroF} Modification
S_{aroF0}	None	None
S_{aroF1}	E274Q	None
S_{aroF2}	N316K	None
S_{aroF3}	E274Q,N316K	None
S_{aroF4}	Δ43	None
S_{aroF5}	Δ93	None
S_{aroF6}	Δ187	None

Fig. 14. Fluorescent output from sensors using P_{aroF}. *E. coli* DJ106 and DJ166 with one of seven sensors consisting of the promoter P_{aroF} and a variant of TyrR were assessed for their fluorescence output (diamonds) based on the amount of tyrosine produced (bars). The table lists each sensor with its constituent variant of TyrR and P_{aroF}.

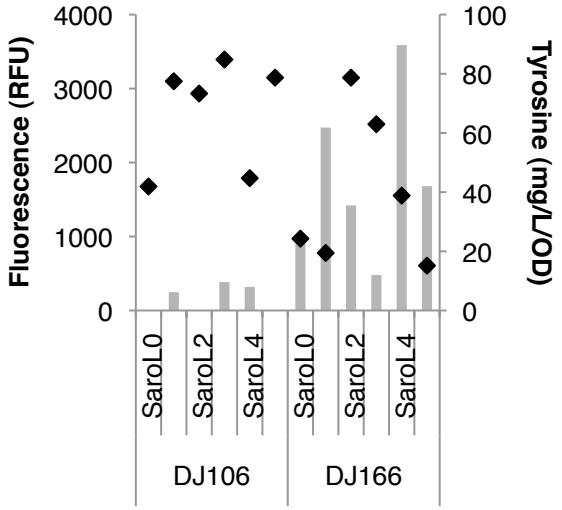

Name	TyrR Modification	P_{aroL} Modification
S_{aroL0}	None	None
S_{aroL1}	E274Q	None
S_{aroL2}	N316K	None
S_{aroL3}	E274Q,N316K	None
S_{aroL4}	None	Box 1 and Box 2
S_{aroL5}	None	Box 3

Fig. 15. Fluorescent output from sensor using P_{aroL}. *E. coli* DJ106 and DJ166 with one of six sensors consisting of a variant of the promoter P_{aroL} and a variant of TyrR were assessed for their fluorescence output (diamonds) based on the amount of tyrosine produced (bars). The table lists each sensor with its constituent variant of TyrR and P_{aroL}.

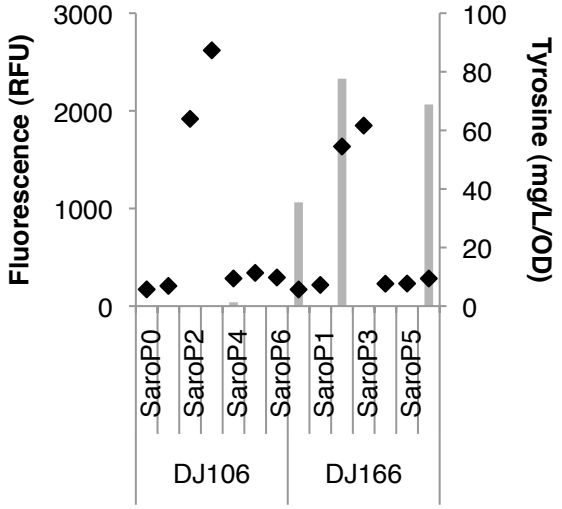

Name	TyrR Modification	P_{aroP} Modification
S_{aroP0}	None	None
S_{aroP1}	E274Q	None
S_{aroP2}	N316K	None
S_{aroP3}	E274Q,N316K	None
S_{aroP4}	None	P_{2UP}
S_{aroP5}	Δ43	P_{2UP}
S_{aroP6}	Δ93	P_{2UP}

Fig. 16. Fluorescent output from sensors using P_{aroP}. *E. coli* DJ106 and DJ166 with one of seven sensors consisting of a variant of the promoter P_{aroP} and a variant of TyrR were assessed for their fluorescence output (diamonds) based on the amount of tyrosine produced (bars). The table lists each sensor with its constituent variant of TyrR and P_{aroP}.

Sensor S_{aroF3} was the most sensitive to changes in tyrosine concentration, showing a 25% decrease in fluorescence from the lower to higher producing strain and a dynamic range of 0.44 RFU/mM/OD (Fig. 17A). We tested FREP implemented with S_{aroF3} for the sensor and *mutD5* for the actuator in *E. coli* DJ238, expressing *mcherry* bicistronically with *mutD5* to monitor T and the relative mutator levels in the cell. We reasoned that *mcherry* levels could decrease in response to either increased tyrosine production or mutations disrupting the sensor or *mcherry* expression. We isolated ten colonies with the lowest

fluorescence after 24 hours and quantified tyrosine production to distinguish between the different scenarios. All ten mutants demonstrated increased tyrosine production, and one exhibited greater than five-fold increase compared to the starting strain (Fig. 17B). Our observations indicate that raising M when L (tyrosine) is low increased tyrosine production, and the higher L increased ΔT, consistent with our design.

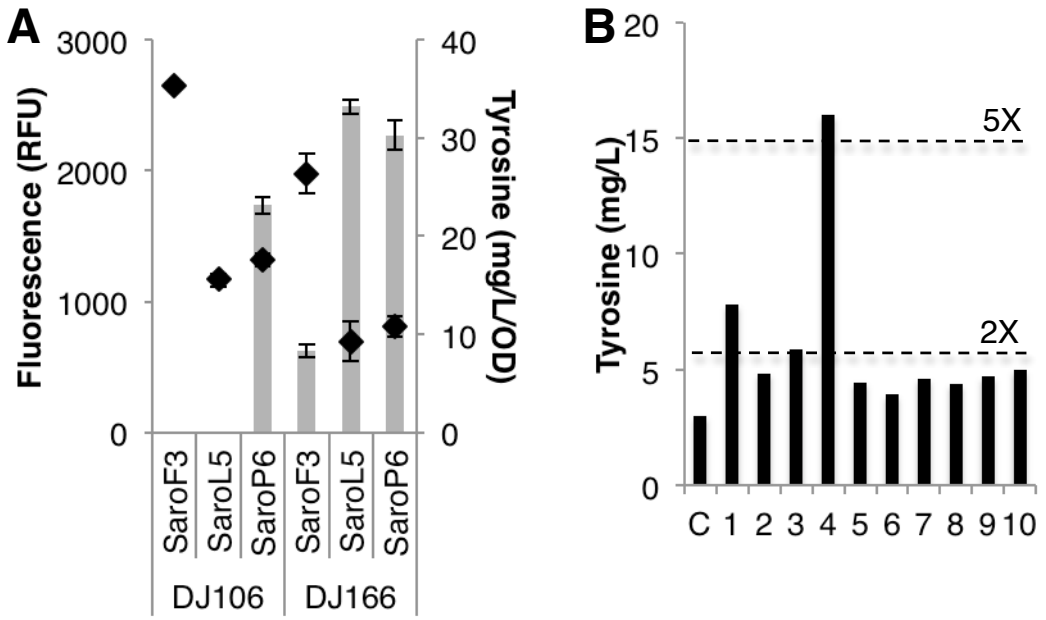

Fig. 17. FREP evolves increased tyrosine production. (**A**) Out of twenty sensors tested, the most sensitive sensors for each promoter (P_{aroF}, P_{aroL}, P_{aroP}) are compared for sensitivity to changes in tyrosine concentration *in vivo*. Bars represent tyrosine production and diamonds represent relative fluorescence units normalized to OD measured at 600 nm. DJ106 and DJ166 are variants of *E. coli* BLR, and DJ166 produces more tyrosine than DJ106. (**B**) Tyrosine production from ten mutants evolved with FREP showing the lowest fluorescence after 24 hours. C is the control not evolved with FREP.

To determine if FREP could evolve other traits, we implemented an adaptive control system to increase production of isoprenoids, a class of compounds with a wide range of industrial applications, such as drugs (70) and biofuels (4). Natural TFs for these compounds have not been discovered yet, so we developed a framework to rationally assemble synthetic TFs that could be used to regulate evolution towards high isoprenoid-producing strains. Our strategy was to construct synthetic TFs reminiscent of natural TFs by taking advantage of their structural and functional modularity. The framework assembles a synthetic TFs from three parts: Part1 binds the target ligand, Part2 converts the binding signal into ΔT by regulating RNA polymerase binding to the target promoter, and Part3 joins Part1 and Part2 together.

For example, AraC regulates expression of arabinose utilization genes from the promoter P_{BAD} by preferentially binding different DNA sequences in the presence and absence of arabinose (71). AraC has a distinct N-terminal, ligand-binding domain (LBD) and C-terminal, DNA-binding domain (DBD), and changes its ability to activate or repress P_{BAD}

depending on whether the LBD has bound arabinose. We reasoned it should be possible to construct synthetic TFs for isoprenoids by replacing AraC's LBD with proteins that bind isoprenoids. We engineered a synthetic *E. coli* TF (chimeric protein IA, Fig. 18A) to respond to isopentenyl diphosphate (IPP), the central intermediate for all isoprenoid biosynthesis (29), by fusing the AraC DBD (Part2) and linker (Part3) with IPP isomerase (*idi* (41)) (Part1). We chose Idi, because crystallographic data indicated that it dimerizes upon binding IPP (72), suggesting that dimerization of Part1 should create at least two, different conformational states for IA, only one of which should activate transcription. A sensor consisting of IA and P_{BAD} was tested by monitoring its output with *mcherry* in a modified strain of *E. coli* MG1655 able to convert mevalonate to IPP (HC175). Titrating mevalonate from 0-10 mM changed fluorescence by over three fold (Fig. 18B).

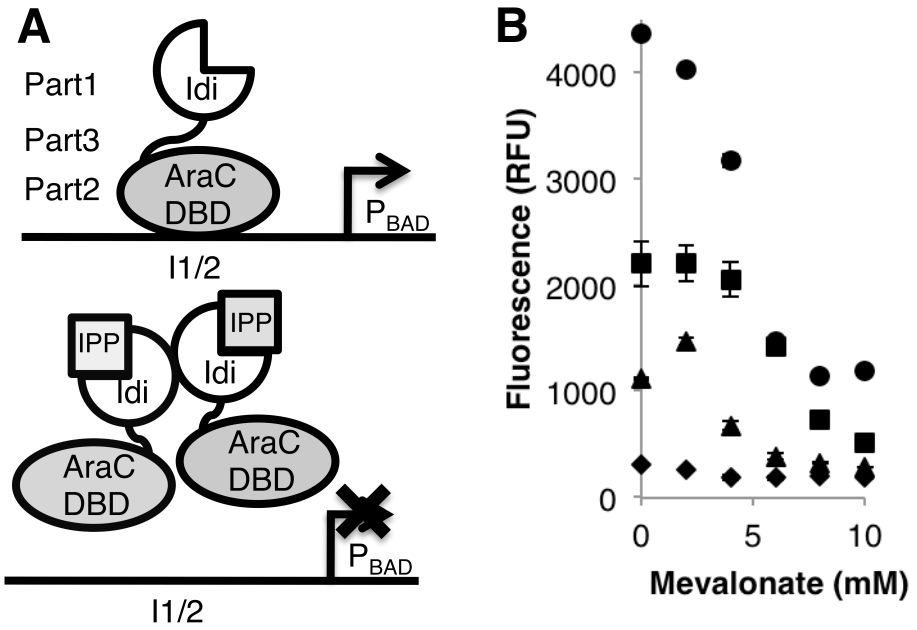

Fig. 18. Bacterial synthetic transcription factors (TFs) respond to IPP. (**A**) A synthetic TF consists of 3 parts: Part1 binds the target ligand, Part2 converts the binding signal into a change in RNA polymerase binding to the target promoter, and Part3 is an amino acid linker fusing Part1 and Part2 together. Here, a sensor with synthetic TF IA comprised of Idi as Part1 and AraC's DBD and linker as Part2 and Part3, respectively. One model for how IA regulates P_{BAD} is IA binds the DNA sequence I_1I_2, activating transcription from P_{BAD} in the absence of IPP (top), and IPP-bound IA dimerizes, preventing binding to I_1I_2 and activation of P_{BAD} (bottom). (**B**) Output of four sensors, each with a different TF, to changing IPP concentrations in *E. coli* HC175 monitored with *mcherry*. Diamonds represent AC, triangles IA32, squares IA, and circles IA44.

There was no change in fluorescence when a synthetic TF consisting of only the AraC DBD and linker (AC) regulated P_{BAD}. We also evaluated expression from the divergent promoter (P_c) with *cfp* (Table 2). Combined with the P_{BAD} data, IA appears to regulate P_{BAD} and P_C nearly as tightly as AraC. Unlike AraC, IA represses P_{BAD} in the presence of ligand. Furthermore, both half-sites I_1 and I_2 upstream of P_{BAD} are necessary but interchangeable for IA regulation (Table 3). These observations indicate IA can regulate

T from P_{BAD} based on L (IPP concentration) with a dynamic range of 210 RFU/mM/OD, assuming all of the mevalonate was converted to IPP.

Table 2. Fluorescence output from P_{BAD} and P_C. The promoters P_{BAD} and P_C were regulated by one of three TFs: AC, AraC, or IA. P_{BAD} was monitored using RFP and P_C with CFP. Fluorescence output was normalized to the output from the promoters regulated by IA in the absence of mevalonate (0 mM). Experiments were performed in HC175 induced with 0.1 mM IPTG. 10 mM arabinose was added in the case of "+ Inducer" for AraC, and 10 mM mevalonate was added in the cases of "+ Inducer" for AC and IA.

	CFP		RFP	
	- Inducer	+ Inducer	- Inducer	+ Inducer
AC	2.8 ± 0.02	1.4 ± 0.2	0.19 ± 0.03	0.11 ± 0.02
AraC	1.5 ± 0.05	0.80 ± 0.03	0.22 ± 0.01	1.5 ± 0.002
IA	1.0 ± 0.06	0.64 ± 0.1	1.0 ± 0.07	0.28 ± 0.1

Table 3. Fluorescence output from P_{BAD} with different regulatory sequences. One of four combinations of the half-sites I_1 and I_2 (shown in bold) was used to regulate expression from P_{BAD}. Fluorescence values were normalized to the output using the wild-type I_1I_2 sequence in the absence of inducer (0 mM mevalonate). Experiments were performed in HC175 induced with 0.1 mM IPTG, and 10 mM mevalonate was added in the case of "+ Inducer".

	Sequence	- Inducer	+ Inducer
I_1I_1	**tagcatttttatccata**agat**tagcatttttatccata**	0.10 ± 0.00	0.13 ± 0.01
I_1I_2	**tagcatttttatccata**agat**tagcggatcctacctga**	1.00 ± 0.02	0.36 ± 0.01
I_2I_1	**tagcggatcctacctga**agat**tagcatttttatccata**	1.12 ± 0.06	0.56 ± 0.01
I_2I_2	**tagcggatcctacctga**agat**tagcggatcctacctga**	0.14 ± 0.01	0.11 ± 0.00

We purified IA to confirm it binds the I_1 and I_2 half-sites adjacent P_{BAD} *in vitro*. Gel electrophoresis mobility shift assay (EMSA (73)) experiments showed two bands when I_1 and I_1I_2 were substrates, and three bands when the substrate was the DNA sequence from P_C to P_{BAD} (Fig. 19). The additional band supports the observation that IA regulates both P_{BAD} and P_C, which have distinct binding sequences. The shifted DNA bands were less intense when IPP was added, indicating that IA's affinity for the binding sequences decreases in the presence of IPP.

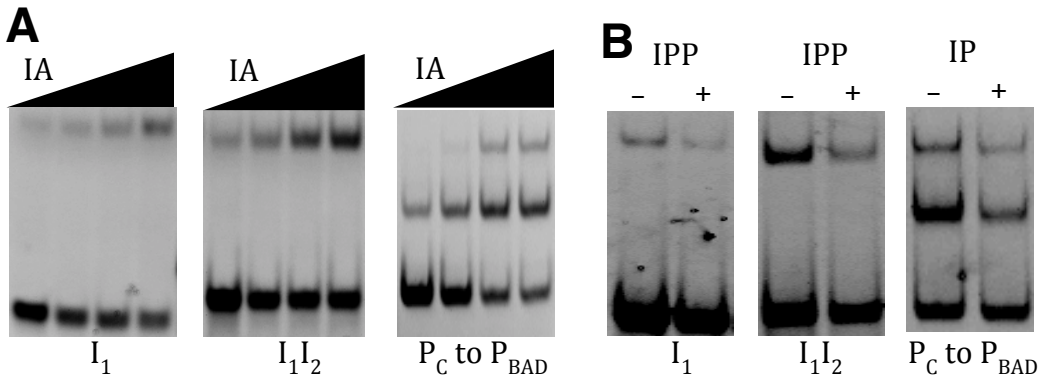

Fig. 19. EMSA experiments show IA binds DNA. We tested whether IA bound to the DNA duplexes of I_1, I_1I_2, or the sequence from P_C to P_{BAD} (20 nM) *in vitro*. (**A**) Increasing IA concentrations (0, 2.5, 5, 10 nM) led to increased intensity in shifted bands. (**B**) IA binding in the presence (+, 10 μM) and absence (-, 0 μM) of IPP with 10 nM of IA.

We confirmed that IPP modulates IA DNA binding using fluorescence resonance energy transfer (FRET) by splitting I_1 and I_1I_2 into two DNA fragments each constituting half of the original sequence and tagged with either a fluorophore or quencher (74). Only the presence of IA and both half-sequences induced a change in fluorescence (Fig. 20).

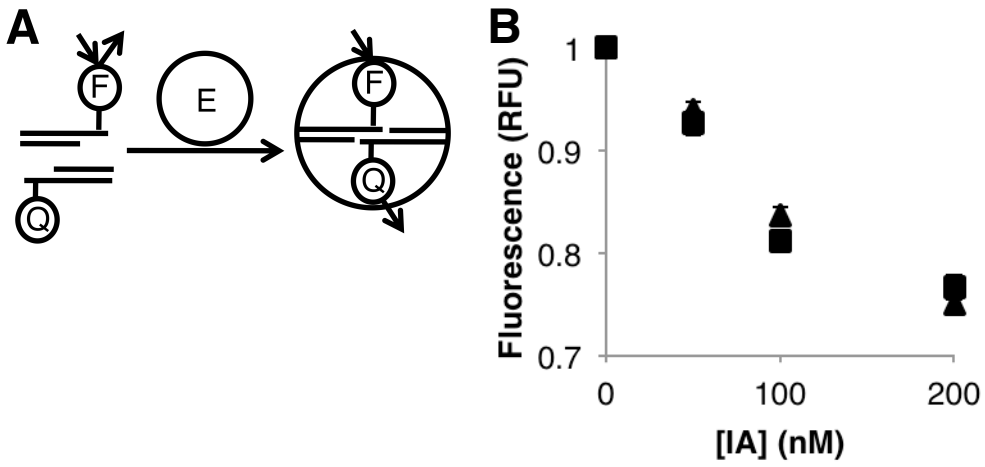

Fig. 20. *In vitro* FRET DNA-binding assay detects IA interacting with DNA. (**A**) Schema illustrating FRET DNA-binding assay. A DNA duplex is split into two half-duplexes, and each half is tagged with either a fluorophore (F) or quencher (Q). Fluorescence is detected in the absence of a protein to bring the two half duplexes together. However, the energy is transferred from F to Q when the protein binds both half sequences and brings F in close enough proximity with Q, leading to a decrease in fluorescence. (**B**) Decreases in fluorescence were observed when the I_1 half-duplex (square, 100 nM; triangle, 200 nM) were incubated with different concentrations of IA (0, 5, 10, and 20 nM). Relative fluorescence values were calculated by subtracting the fluorescence value of the negative control without the F label and dividing by the fluorescence value from 0 nM IA.

Adding IPP decreased the change in fluorescence across all concentrations of IA tested (Fig. 21). Thus, both *in vivo* and *in vitro* data are consistent with IA regulation of transcription from P_{BAD} according to changing IPP concentrations, and both I_1 and I_2 half-sites are necessary for this regulation.

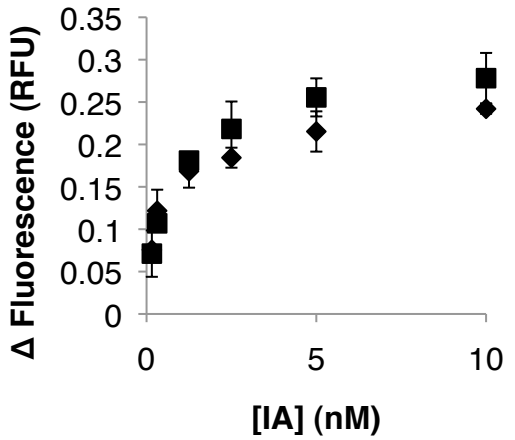

Fig. 21. *In vitro* FRET DNA-binding assay detects that IPP affects IA binding to DNA. We incubated different concentrations of IA with 100 nM of each I_1I_2 labeled DNA half-duplex *in vitro*. A greater change in fluorescence was observed with increasing concentrations of IA, consistent with the binding experiment with I_1 half-duplexes as substrate. The change in fluorescence decreased in the presence of IPP (diamond, 500 nM) compared to when no IPP was added (square, 0 nM).

To demonstrate that our framework for assembling synthetic TFs could be generalized to other organisms, we constructed a synthetic TF for isoprenoids in *Saccharomyces cerevisiae* using the GAL4 protein, which regulates expression of GAL genes in response to galactose (75). Similar to AraC, the functional domains of GAL4 are structurally distinct, consisting of an activator domain (AD) and DBD (76). We reused Idi as Part1 and fused it to the GAL4 AD and DBD (Part2), reasoning that Idi dimerization should bring the AD and DBD in close enough proximity to activate transcription from a GAL promoter (e.g., P_{GAL10}). Part3 was a 19-amino acid sequence having relatively high stability (33). This sensor (Fig. 22A) was tested by monitoring its output with the fluorescent protein yEcitrine in *S. cerevisiae* MO219, a genetically modified strain that increases isoprenoid production when induced with galactose (11). We observed a change in fluorescence greater than baseline after galactose induction (Fig. 22B). Two additional yeast TFs were constructed from yeast proteins known to bind IPP (Idi1 (77) and Erg20 (78)) as Part1 in place of Idi, and both showed even greater changes in fluorescence following induction. Induction led to an almost two-fold increase in sensor output in response to increased isoprenoid levels using the synthetic TF constructed with Erg20. Combined with IA, these GAL4-based TFs highlight our design's modularity in assembling synthetic TFs for constructing sensors, alleviating the need to rely on pre-existing biological components.

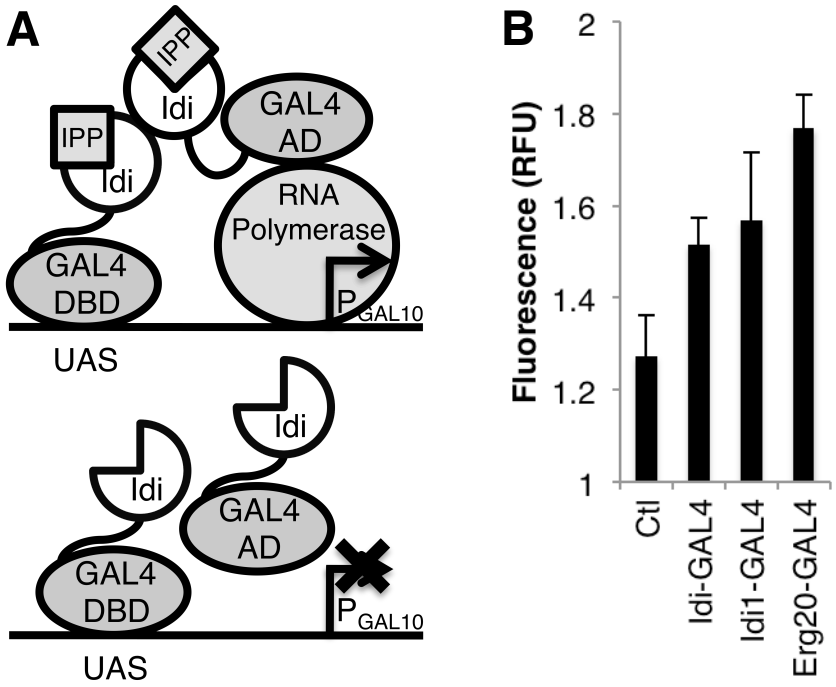

Fig. 22. Yeast synthetic transcription factors (TFs) responds to IPP. (**A**) A sensor for detecting IPP in *S. cerevisiae*. The synthetic TF consists of Idi as Part1, GAL4's AD and DBD as Part2, and a 19-amino acid linker as Part3. One model for P_{GAL10} regulation is that Idi dimerizes when bound to IPP, bringing the upstream activation sequence (UAS)-bound GAL4 DBD in close enough proximity with the GAL4 AD to activate transcription (top). In the absence of Part1 dimerization, there is no transcription from P_{GAL10} (bottom). (**B**) P_{GAL10} output from three sensors with synthetic TFs in *S. cerevisiae* MO219 induced with galactose. The synthetic TFs consist of Idi, Idi1, or Erg20 as Part1 fused to GAL4's AD and DBD. Ctl is the control without synthetic TFs. Output was monitored with the fluorescent protein yEcitrine and normalized to fluorescence in the absence of galactose.

Next, we modified the *E. coli* IPP TF IA using error-prone PCR to create IPP sensors with different dynamic ranges and maximum transcription levels (T_{max}). Out of the 60 variants screened (Fig. 23), IA32 (L39M, S127C) showed half the T_{max} of IA and a dynamic range of 145 RFU/mM/OD, while IA44 (R267H) showed twice the T_{max} of IA and a dynamic range of 350 RFU/mM/OD (Fig. 18B).

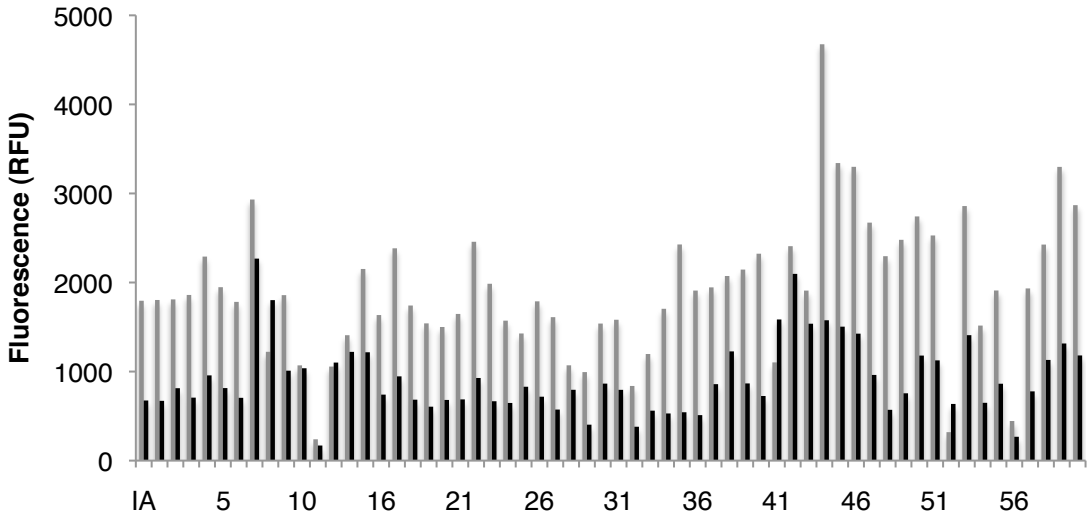

Fig. 23. Modified IPP sensors exhibit different dynamics. 60 different sensors for IPP were generated by mutating IA using error-prone PCR and monitoring sensor output from P_{BAD} with mcherry. Output is presented in relative fluorescence units normalized to OD measured at 600 nm. Gray bars indicate output in the absence of mevalonate (0 mM), and black bars indicate output in the presence of mevalonate (10 mM). A control sensor with IA is included on the left.

We implemented FREP using one of three synthetic TFs (AC, IA32, or IA44) as part of the sensor and the *mutD5* actuator, and examined these constructs in *E. coli* MG1655 using Luria-Delbruck fluctuation analysis (79). Thirty colonies for each implementation were tested for rifampicin resistance, an orthogonal phenotype that could be quantified quickly. In general, we observed more rifampicin-resistant mutants with higher mutator expression, and a strong correlation between relative mutator expression and mutation rate (r=0.97) (Fig. 24). For example, IA32 and IA44 exhibited a four-fold difference in T_{max} and a 2.4-fold difference in M. A negative control consisting of a sensor with IA44 and no actuator generated no rifampicin-resistant mutants. These results show that increasing ΔT decreases M, consistent with our design, and suggest that dynamically controlling mutator expression changes mutation rates.

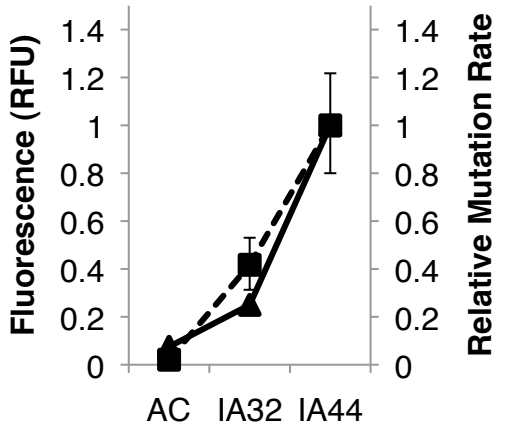

Fig. 24. Fluorescence output and mutation rate correlate. FREP was implemented with the *mutD5* mutator and an IPP sensor with one of the following TFs: AC, IA32, or IA44. Fluorescence (triangle) represents the maximum fluorescence measured from HC175 in the absence of mevalonate for each sensor normalized to that with IA44 (Figure 3B). The mutation rate (square) was calculated with Luria-Delbruck analysis using rifampicin resistance as the phenotype, analyzed using FALCOR, and the mutation rate for each TF determined by FALCOR was normalized to that determined for IA44. The correlation coefficient between measured fluorescence and mutation rate is r=0.97.

We performed FREP with IA44 to increase isoprenoid production in *E. coli* MG1655, and expressed *mcherry* bicistronically with the actuator to monitor relative mutation rates. Ten colonies with the lowest fluorescence after 24 hours were made electrocompetent and transformed with a plasmid containing the lycopene synthase genes (pLyc). Lycopene measured from a random transformant for all ten colonies was higher than the control not modified with FREP. Six colonies had mutants producing on average 2900 μg lycopene/g dry cell weight (p.p.m.), a nearly three-fold increase compared to the control that did not undergo FREP, which produced only 1000 p.p.m. (Fig. 25). Repeating the experiment with a sensor employing AraC as a negative control (AraC does not respond to IPP) generated no mutants producing more lycopene than the initial strain, illustrating the importance of the feedback loop between M and L to couple the mutation rate to the phenotype being evolved.

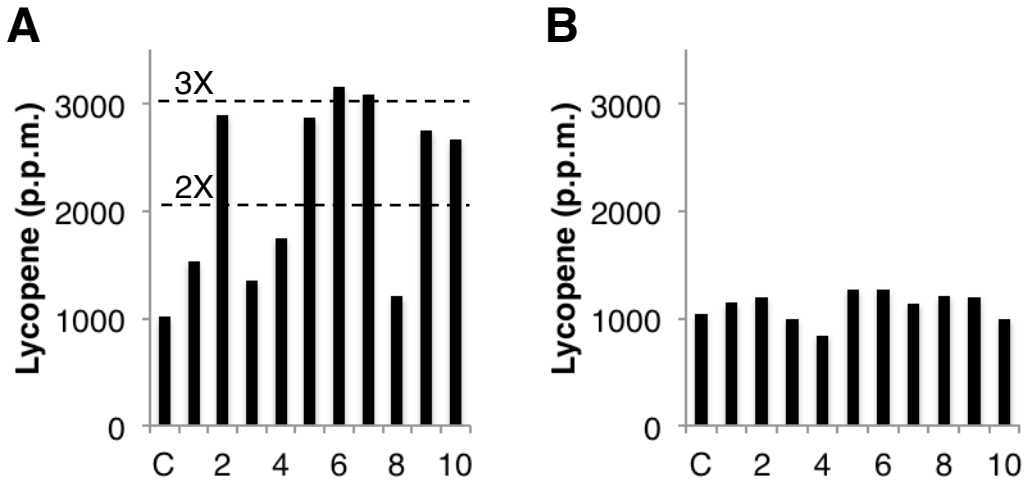

Fig. 25. FREP evolves increased IPP production in 24 hours. C is the negative control that did not undergo FREP. (A) The effects of dynamic control of mutation rate was determined by comparing lycopene production from C to 10 colonies of *E. coli* MG1655 after undergoing FREP with IA44 for 24 hours. (B) The effects of static control of mutation rate was determined by comparing lycopene production from C to 10 colonies of *E. coli* MG1655 after undergoing FREP with AraC induced with 10 mM arabinose for 24 hours.

Finally, we examined the ability of FREP to generate novel phenotypes in the context of a long-term experiment. We co-transformed pLyc with an IPP sensor and *mutD5* actuator into *E. coli* MG1655, and monitored the evolution of IPP production using lycopene as a reporter over 432 hours. We quantified lycopene production every 72 hours from ten random colonies and only passaged the isolate demonstrating the highest

production levels. After 432 hours, lycopene production increased to 6800 p.p.m. using IA44, 4700 p.p.m. using IA32, and only 400 p.p.m. using AraC (Fig. 26). A negative FREP control implemented with IA44 without an actuator produced 0 p.p.m.

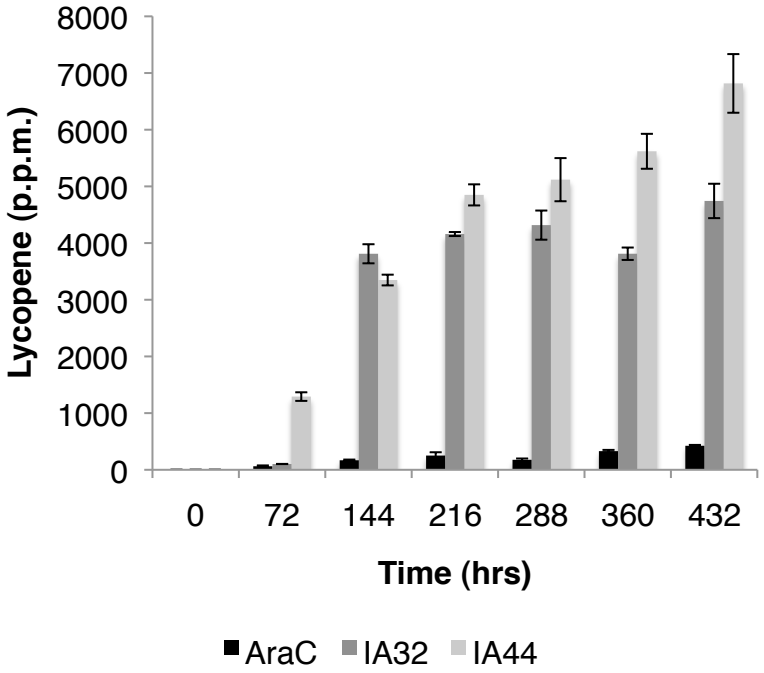

Fig. 26. FREP evolves increased IPP production in long-term experiment. Lycopene production sampled every 72 hours over a 432-hour period from *E. coli* MG1655 expressing pLyc, an IPP sensor, and an actuator. The transcription factors used in the sensor were AraC (black bars), IA32 (dark gray bars), or IA44 (light gray bars). Lycopene production is presented as p.p.m. (ug/g dry cell weight). The sensor with AraC was induced with 10 mM arabinose.

For the strains evolved using FREP implemented with IA44 and an actuator, we purified pLyc from each time point. Transforming those plasmids into *E. coli* MG1655 did not lead to more lycopene production compared to the original plasmid (Fig. 27). This observation indicates that mutations generated by FREP that increase isoprenoid production reside on the chromosome and are specific to increasing IPP production.

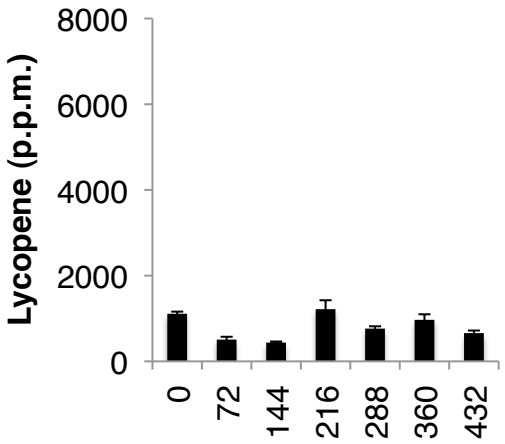

Fig. 27. pLyc from mutants do not lead to increased lycopene production. pLyc was isolated from *E. coli* MG1655 after undergoing FREP for 0, 72, 144, 216, 288, 360, and 432 hours. The plasmids were transformed into *E. coli* MG1655 and lycopene production was quantified.

Overall, our data demonstrate that dynamical control of the mutation rate evolved a particular phenotype faster than either the absence of or static control of the mutation rate, and the beneficial mutations generated by the dynamic control process are specific to the desired phenotype.

Discussion

We successfully designed and implemented an adaptive control process capable of regulating the mutation rate by gauging the degree to which a strain exhibits a desired phenotype. Unlike existing methods to engineer metabolism (80, 81), FREP has the advantage of not requiring *a priori* knowledge about the genes, RNA, proteins, and their interactions that govern the trait being evolved. This approach is distinct from other directed evolution approaches requiring phenotype-specific, high-throughput screens or selections to identify high-performing mutants.

We demonstrated the application of FREP by evolving *E. coli* to increase tyrosine and IPP production, and isolating the evolved strains by monitoring the actuator level with a fluorescent protein. We confirmed that FREP was able to evolve phenotypes for target ligands that are permeable (tyrosine) and for those that are impermeable (IPP) to the cell membrane. Additionally, we presented a framework to rationally construct synthetic TFs that enable the development of orthogonal sensors less likely to interact with existing cellular networks without being limited to the molecular recognition properties and control functions of naturally occurring TFs.

More broadly, this approach to sensor engineering may have applications in anti-viral therapeutics, gene therapy, and stem cell reprogramming, where tight regulation of complicated, spatio-temporal, intracellular interactions are necessary (82, 83). Above all, our work provides a foundation for assembling intelligent, synthetic biological systems

capable of autonomously making decisions by incorporating real-time, intra- and extracellular information.

Chapter 5: Conclusions and Future Directions

There is a growing need to replace industrial processes that use nonrenewable petroleum feedstock and practices that damage the environment with new processes that are more sustainable and environmentally friendly. This change is necessary for the sustainable growth of established, as well as new and growing economies. Many different solutions are concurrently being developed as companies slowly embrace the new technologies that enable the transition towards more sustainable practices. One of these solutions is the development of bioprocesses to convert renewable carbon feedstock into industrial products currently produced from petroleum.

Two major challenges in the development of bioprocesses are the design and implementation of new biological processes to synthesize a desired product, and the optimization of a process to achieve higher titers. The products synthesized from renewable feedstock using new bioprocesses must either substitute or replace existing products manufactured using petroleum feedstock in order to decrease the reliance on petroleum. The optimization of the new bioprocesses to achieve higher titers is necessary for competing with petroleum-based processes and achieving economic viability. Here, we described frameworks addressing these two challenges and provided examples illustrating the implementation of these frameworks.

In Chapter 2, I proposed a framework using enzyme families as libraries to identify enzymes able to catalyze a desired reaction. Using the framework, I identified seven enzymes in *E. coli* from the HAD-like phosphatase and Nudix hydrolase families that are able to catalyze a novel phosphatase reaction using IPP and DMAPP as substrates. Furthermore, I identified one enzyme in *E. coli* from the Old Yellow Enzyme family able to catalyze a novel reductase reaction using 3-methyl-2-butenol as a substrate. Neither of these reactions exists in nature. I also engineered two synthetic bifunctional enzymes that compete with the native enzymes in *E. coli* for IPP and redirect flux towards the synthetic pathway for the production of five-carbon alcohols. Taken together, these enzymes were assembled into a novel synthetic pathway that produces 3-methyl-3-butenol, 3-methyl-2-butenol, and 3-methyl-butanol from IPP. Unlike previous work in assembling synthetic biological pathways, I constructed a synthetic pathway using only genes from the production host. Enzyme expression and function in a heterologous host are sometimes problematic during metabolic engineering and cannot always be solved using standard techniques, such as codon optimization. Therefore, one of the advantages of using enzymes from the production host is that the enzymes are guaranteed to express and function properly. This framework could be used to quickly assemble many different synthetic biological pathways to produce existing and new chemicals that could replace petroleum-based products.

In Chapter 3, I described a new colorimetric assay for 3-methyl-3-butenol, 3-methyl-2-butenol, and 3-methyl-butanol. The assay was demonstrated to work in a 96-well format, so its automation would enable the development of a high-throughput assay for these three five-carbon alcohols. Currently, the quantification of these three alcohols is performed using GC, limiting the throughput to 10^2 samples/instrument/day. Automation

of the MBTH assay would increase the throughput up to 10^4 samples/instrument/day. The increase in throughput would enable larger libraries of mutants to be quickly screened for increased five-carbon alcohol production, and accelerate the engineering of a strain that could be used to produce five-carbon alcohols from IPP economically at commercial scale in the future.

In Chapter 4, I proposed two frameworks that could be used together to increase the production of any small molecule. The FREP framework is an adaptive control system that controls the mutation rate based on the level of a particular phenotype. I verified FREP by implementing a system that increased tyrosine production in *E. coli*. The second framework describes a method using metabolic enzymes to construct synthetic transcription factors that can sense the concentration of a desired small molecule and generate a transcriptional change based on its concentration. The combination of the two frameworks enabled the implementation of a system to dynamically regulates the mutation rate based on the IPP concentration inside the cell and led to increased IPP production. Unlike the traditional approaches to directed evolution that perform the mutagenesis and screening/selection steps separately, the approach I described here performs both steps *in vivo* as a single-step process (e.g., mutagenesis and selection happens concurrently inside the cell, and mutagenesis stops once the desired phenotype level is achieved). The FREP framework could be used to evolve other phenotypes essential for producing chemicals from renewable feedstock, such as the increased utilization of new carbon sources, increased tolerance towards growth inhibitors found in the bioprocess, and increased productivity and yields of the target chemical. The framework for building synthetic transcription factors could be used in the cases where a natural transcription factor does not exist for the phenotype being evolved using FREP.

Overall, this work provides three new tools for addressing the challenges of designing, assembling, and optimizing biological pathways. The tools are 1) using enzyme families as libraries for identifying enzymes to catalyze novel reactions, 2) FREP, and 3) constructing synthetic transcription factors from metabolic enzymes. I have demonstrated how these three tools could be useful for engineering bioprocesses for the conversion of renewable biomass feedstock into commercially important chemicals currently derived from petroleum feedstock.

References

1. Wyman CE. 1994. Ethanol from Lignocellulosic Biomass: Technology, Economics, and Opportunities. Bioresource Technology **50:**3-16.
2. Lee SK, Chou H, Ham TS, Lee TS, Keasling JD. 2008. Metabolic engineering of microorganisms for biofuel production: from bugs to synthetic biology to fuels. Current Opinion in Biotechnology **19:**556-563.
3. Fortman JL, Chhabra S, Mukhopadhyay A, Chou H, Lee TS, Steen E, Keasling JD. 2008. Biofuel alternatives to ethanol: pumping the microbial well. Trends in Biotechnology **26:**375-381.
4. Keasling JD, Chou H. 2008. Metabolic engineering delivers next-generation biofuels. Nature Biotechnology **26:**298-299.
5. Chou HH, Keasling JD. July 2011. Host Cells and Methods for Producing 3-Methyl-2-buten-1-ol, 3-Methyl-3-buten-1-ol, and 3-Methyl-butan-1-ol. Patent No. 7,985,567.
6. Lee SK, Chou HH, Pfleger BF, Newman JD, Yoshikuni Y, Keasling JD. 2007. Directed Evolution of AraC for Improved Compatibility of Arabinose- and Lactose-Inducible Promoters. Applied and Environmental Microbiology **73:**5711-5715.
7. Keasling JD. 2010. Manufacturing Molecules Through Metabolic Engineering. Science **330:**1355-1358.
8. Villadsen J, Nielsen J, Liden G. 2011. Chemicals from Metabolic Pathways, p. 7-62. *In* Bioreaction and Engineering Principles, 3rd ed. Springer-Verlag, New York, NY.
9. Martin VJ, Pitera DJ, Withers ST, Newman JD, Keasling JD. 2003. Engineering a mevalonate pathway in *Escherichia coli* for production of terpenoids. Nature Biotechnology **7:**796-802.
10. Steen EJ, Chan R, Prasad N, Myers S, Petzold CJ, Redding A, Ouellet M, Keasling JD. 2008. Metabolic engineering of *Saccharomyces cerevisiae* for the production of n-butanol. Microb. Cell Fact. **7:**36.
11. Ro D-K, Paradise EM, Ouellet M, Fisher KJ, Newman KL, Ndungu JM, Ho KA, Eachus RA, Ham TS, Kirby JK, Chang MCY, Withers ST, Shiba Y, Sarpong R, Keasling JD. 2006. Production of the antimalarial drug precursor artemisinic acid in engineered yeast. Nature **440:**940-943.
12. Zhang K, Sawaya MR, Eisenberg DS, Liao JC. 2008. Expanding metabolism for biosynthesis of nonnatural alcohols. Proc. Natl. Acad. Sci. USA **105:**20653-20658.
13. Moon, TS, Yoon S-H, Lanza AM, Roy-Mayhew JD, Prather, KLJ. 2009. Production of Glucaric Acid from a Synthetic Pathway in Recombinant *Escherichia coli*. Applied and Environmental Microbiology **75:**589-595.
14. Steen EJ, Kang Y, Bokinsky G, Hu Z, Schirmer A, McClure A, del Cardayre SB, Keasling JD. 2010. Microbial production of fatty-acid-derived fuels and chemicals from plant biomass. Nature **463:**559-562.
15. Wargacki AJ, Leonard E, Win MN, Regitsky DD, Santos CNS, Kim PB, Cooper SR, Raisner RM, Herman A, Sivitz AB, Lakshmanaswamy A, Kashiyama Y, Baker D, Yoshikuni Y. 2012. An Engineered Microbial Platform for Direct Biofuel Production from Brown Microalgae. Science **335:**308-313.
16. Kazlauskas RJ, Bornscheuer UT. 2009. Finding better protein engineering strategies. Nature Chemical Biology **5:**526-529.

17. Siegel JB, Zanghellini A, Lovick HM, Kiss G, Lambert AR, St.Clair JL, Gallaher JL, Hilvert D, Gelb MH, Stoddard BL, Houk KN, Michael FE, Baker D. 2010. Computational design of an enzyme catalyst for a stereoselective biomolecular Diels-Alder reaction. Science **329:**309-313.
18. Jensen RA. 1976. Enzyme Recruitment in Evolution of New Function. Annu. Rev. Microbio. **30:**409-425.
19. Babbitt PC, Gerlt JA. 1997. Understanding enzyme superfamilies. Chemistry as the fundamental determinant in the evolution of new catalytic activities. Journal of Biological Chemistry **272:**30591-30594.
20. Chiang RA, Sali A, Babbitt PC. 2008. Evolutionarily Conserved Substrate Substructures for Automated Annotation of Enzyme Superfamilies. PLoS Computational Biology **4:**e1000142.
21. Russell RJ, Scott C, Jackson CJ, Pandey R, Pandey G, Taylor MC, Coppin CW, Liu J-W, Oakeshott JG. 2011. The evolution of new enzyme function: lessons from xenobiotic metabolizing bacteria versus insecticide-resistant insects. Evolutionary Applications **4:**225-248.
22. Bornscheuer UT, Kazlauskas RJ. 2004. Catalytic Promiscuity in Biocatalysis: Using Old Enzymes to Form New Bonds and Follow New Pathways. Angew. Chem. Int. Ed. **43:**6032-6040.
23. Khersonsky O, Roodveldt C, Tawfik DS. 2006. Enzyme promiscuity: evolutionary and mechanistic aspects. Current Opinion in Chemical Biology **10:**498-508.
24. Prof. Robert Dibble, Department of Mechanical Engineering, University of California, Berkeley, personal communication.
25. Yang Y, Dec J, Dronniou N, Simmons B. 2010. Characteristics of Isopentanol as a Fuel for HCCI Engines. SAE Int. J. Fuels. Lubr. **3:**725-741.
26. Babler JH. August 2001. Methods for Conversion of Isoprene to Prenyl Alcohol and Related Compounds. U.S. patent 6,278,016.
27. Connor MR, Liao JC. 2008. Engineering of an *Escherichia coli* Strain for the Production of 3-methyl-1-Butanol. Applied and Environmental Microbiology **74:** 5769-5775.
28. Hazelwood LA, Daran J-M, van Maris AJA, Pronk JT, Dickinson JR. 2008. The Ehrlich Pathway of Fusel Alcohol Production: a Century of Research on *Saccharomyces cerevisiae* Metabolism. Applied and Environmental Microbiology **74:**2259-2266.
29. Lange BM, Rujan T, Martin W, Croteau R. 2000. Isoprenoid biosynthesis: The evolution of two ancient and distinct pathways across genomes. Proc. Natl. Acad. Sci. USA **97:**13172-13177.
30. Pitera DJ, Paddon CJ, Newman JD, Keasling JD. 2007. Balancing a heterologous mevalonate pathway for improved isoprenoid production in *Escherichia coli*. Metabolic Engineering **9:**193-207.
31. Ajikumar PK, Xiao W-H, Tyo KEJ, Wang Y, Simeon F, Leonard E, Mucha O, Phon TH, Pfeifer B, Stephanopoulos G. 2010. Isoprenoid Pathway Optimization for Taxol Precursor Overproduction in *Escherichia coli*. Science **330:**70-74.
32. Lee SK, Keasling JD. 2008. Heterologous protein production in *Escherichia coli* using the propionate-inducible pPro system by conventional and auto-induction methods. Protein Expression and Purification **61:**197-203.

33. Robinson CR, Sauer RT. 1998. Optimizing the stability of single-chain proteins by linker length and composition mutagenesis. Proc. Natl. Acad. Sci. USA **95:**5929-5934.
34. Burroughs AM, Allen KN, Dunaway-Mariano D, Aravind L. 2006. Evolutionary Genomics of the HAD Superfamily: Understanding the Structural Adaptations and Catalytic Diversity in a Superfamily of Phosphoesterases and Allied Enzymes. J. Mol. Biol. **361:**1003-1034.
35. Mildvan AS, Xia Z, Azurmendi HF, Saraswat V, Legler PM, Massiah MA, Gabelli SB, Bianchet MA, Kang L-W, Amzel LM. 2005. Structures and mechanisms of Nudix hydrolases. Archives of Biochemistry and Biophysics **433:**129-143.
36. Glaner ME, Gerlt JA, Babbitt PC. 2006. Evolution of enzyme superfamilies. Current Opinion in Chemical Biology **10:**492-497.
37. Kuznetsova E, Proudfoot M, Gonzalez CF, Brown G, Omelchenko MV, Borozan I, Carmel L, Wolf YI, Mori H, Savchenko AV, Arrowsmith CH, Koonin EV, Edwards AM, Yakunin AF. 2006. Genome-wide Analysis of Substrate Specificities of the *Escherichia coli* Haloacid Dehalogenase-like Phosphatase Family. Journal of Biological Chemistry **281:**36149-36161.
38. McLennan AG. 2006. The Nudix hydrolase superfamily. Cellular and Molecular Life Sciences **63:**123-143.
39. Withers ST, Gottlieb SS, Lieu B, Newman JD, Keasling JD. 2007. Identification of Isopentenol Biosynthesis Genes from *Bacillus subtilis* by a Screening Method Based on Isoprenoid Precursor Toxicity. Applied and Environmental Microbiology **73:**6277-6283.
40. Hanes JW, Johnson KA. 2008. Real-time measurement of pyrophosphate release kinetics. Analytical Biochemistry **372:**125-127.
41. Hahn FM, Hurlburt AP, Poulter CD. 1999. *Escherichia coli* Open Reading Frame 696 Is *idi*, a Nonessential Gene Encoding Isopentenyl Diphosphate Isomerase. Journal of Bacteriology **181:**4499-4504.
42. Pettersson G. 1989. Effect of evolution on the kinetic properties of enzymes. Eur. J. Biochem. **184:**561-566.
43. Williams RE, Bruce NC. 2002. 'New uses for an Old Enzyme' – the Old Yellow Enzyme family of flavoenzymes. Microbiology **148:**1607-1614.
44. Williams RE, Rathbone DA, Scrutton NS, Bruce NC. Biotransformation of Explosives by the Old Yellow Enzyme Family of Flavoproteins. Applied and Environmental Microbiology **70:**3566-3574.
45. Miura K, Tomioka Y, Suzuki H, Yonezawa M, Hishinuma T, Mizugaki M. Molecular cloning of the *nemA* gene encoding N-ethylmaleimide reductase from *Escherichia coli*. Biol. Pharm. Bull. 20*:*110-112.
46. Fujisaki S, Hara H, Nishimura Y, Horiuchi K, Nishino T. 1990. Cloning and nucleotide sequence of the ispA gene responsible for farnesyl diphosphate synthase activity in *Escherichia coli*. J. Biochem **108:**995-1000.
47. Zhu X, Tang G, Galili G. 2002. The activity of the *Arabidopsis* bifunctional lysine-ketoglutarate reductase/saccaropine dehydorgenase enzyme of lysine catabolism is regulated by functional interaction between its two enzyme domains. J. Biol. Chem. **277:**49655-49661.

48. Bulock KG, Beardsley GP, Anderson KS. 2002. The kinetic mechanism of the human bifunctional enzyme ATIC (5-amino-4-imidazolecarboxamide ribonucleotide transformylase/inosine 5'-monophosphate cyclohydrolase). A surprising lack of substrate channeling. J. Biol. Chem. 277:22168-22174.
49. Peters RJ, Ravn MM, Coates RM, Croteau RB. 2001. Bifunctional abietadiene synthase: free diffusive transfer of the (+)-copalyl diphosphate intermediate between two distinct active sites. J. Am. Chem. Soc. **123:**8974 – 8978.
50. Miron D, Ben-Yaacov S, Reches D, Schupper A, Galili G. 2000. Purification and characterization of bifunctional lyzine- ketoglutarate reductase/saccharopine dehydrogenase from developing soybean seeds. Plant Physiol. **123:**655 – 663.
51. Wriggers W, Chakravarty S, Jennings PA. 2005. Control of Protein Functional Dynamics by Peptide Linkers. Biopolymers **80:**736-746.
52. Street IP, Poulter CD. 1990. Isopentenyl diphosphate:dimethylallyl diphosphate isomerase: construction of a high-level heterologous expression system for the gene from *Saccharomyces cerevisiae* and identification of an active-site nucleophile. Biochemistry **29:**7531-7538.
53. Adam P, Hecht S, Eisenreich W, Kaiser J, Grawert T, Arigoni D, Bacher A, Rohdich F. 2002. Biosynthesis of terpenes: studies on 1-hydroxy-2-methyl-2-(*E*)-butenyl 4-diphosphate reductase. Proc. Natl. Acad. Sci. USA **99:**12101-12113.
54. Street IP, Chistensen DJ, Poulter CD. 1990. Hydrogen exchange during the enzyme catalyzed isomerization of isopentenyl diphosphate and dimethylallyl diphosphate, J. Am. Chem. Soc. **112:**8577-8578.
55. Elena SF, Cooper VS, Lenski RE. 1996. Punctuated Evolution Caused by Selection of Rare Beneficial Mutations. Science **272:**1802-1804.
56. Desai MM, Fisher DS. 2011. The Balance Between Mutator and Nonmutators in Asexual Populations. Genetics **188:**997-1014.
57. Barrick JE, Yu DS, Yoon SH, Jeong H, Oh TK, Schneider D, Lenski RE, Kim JF. 2009. Genome evolution and adaptation in a long-term experiment with *Escherichia coli*. Nature **461:**1243-1247.
58. Sniegowski PD, Gerrish PJ, Lenski RE. 1997. Evolution of high mutation rates in experimental populations of *E. coli*. Nature **387:**703-705.
59. Stich M, Manrubia SC, Lázaro E. 2010. Variable Mutation Rates as an Adaptive Strategy in Replicator Populations. *PLoS ONE* **5:**e11186.
60. Giruad A, Matic I, Tenaillon O, Clara A, Radman M, Fons M, Taddei F. 2001. Costs and Benefits of High Mutation Rates: Adaptive Evolution of Bacteria in the Mouse Gut. Science **291:**2606-2608.
61. Loh E, Salk JJ, Loeb LA. 2010. Optimization of DNA polymerase mutation rates during bacterial evolution. Proc. Natl. Acad. Sci. USA **107:**1154-1159.
62. Dietrich JA, McKee AE, Keasling JD. 2010. High-Throughput Metabolic Engineering: Advances in Small-Molecule Screening and Selection. Annual Review Biochemistry **79:**563-590.
63. Kazlauskas RJ, Bornscheuer UT. 2009. Finding better protein engineering strategies. Nature Chemical Biology **5:**526-529.
64. Greener A, Callahan M, Jerpseth B. 1997. An efficient random mutagenesis technique using an *E. coli* mutator strain. Molecular Biotechnology **7:**188-195.

65. Portnoy VA, Bezdan D, Zengler K. 2011. Adaptive laboratory evolution – harnessing the power of biology for metabolic engineering. Current Opinion in Biotechnology **22:**590-594.
66. Astrom KJ. 1987. Adaptive Feedback Control. Proceedings of the IEEE **75:**185-217.
67. Juminaga D, Baidoo, EEK, Redding-Johanson AM, Batth TS, Burd H, Mukhopadhyay A, Petzold CJ, Keasling JD. *2012*. Modular Engineering of *L*-Tyrosine Production in *Escherichia coli*. Applied and Environmental Microbiology **78:**89-98.
68. Pittard J, Camakaris H, Yang J. 2005. The TyrR regulon. Molecular Microbiology **55:**16-26.
69. Schaaper RM. 1988. Mechanisms of mutagenesis in the *Escherichia coli* mutator *mutD5*: Role of DNA mismatch repair. Proc. Natl. Acad. Sci. USA **85:**8126-8130.
70. Chang MCY, Keasling JD. 2006. Production of isoprenoid pharmaceuticals by engineered microbes. Nature Chemical Biology **2:**674-681.
71. Soisson SM, MacDougall-Shackleton B, Schleif R, Wolberger C. 1997. Structural Basis for Ligand-Regulated Oligomerization of AraC. Science **276:**421-425.
72. De Ruyck J, Oudjama Y, Wouters J. 2008. Monoclinic form of isopentenyl diphosphate isomerase: a case of polymorphism in biomolecular crystals. Acta. Cryst. **F64:**239-242.
73. Hellman LM, Fried MG. 2007. Electrophoretic mobility shift assay (EMSA) for detecting protein-nucleic acid interactions. Nature Protocols **2:**1849-1861.
74. Heyduk T, Heyduk E. 2002. Molecular beacons for detecting DNA binding proteins. Nature Biotechnology **20:**171-176.
75. Traven A, Jelicic B, Sopta M. 2006. Yeast Gal4: a transcriptional paradigm revisited. EMBO **7:**496-499.
76. Fields S, Song O-k. 1989. A novel genetic system to detect protein-protein interactions. Nature **340:**245-246.
77. Mayer MP, Hahn FM, Stillman DJ, Poulter CD. 1992. Disruption and mapping of IDI, the gene for isopentenyl diphosphate isomerase in *Saccharomyces cerevisiae*. Yeast **8:**743-748.
78. Fischer MJ, Meyer S, Claudel P, Bergdoll M, Karst F. 2011. Metabolic Engineering of Monoterpene Synthesis in Yeast. Biotechnology and Bioengineering **108:**1883-1892.
79. Rosche WA, Foster PL. 2000. Determining Mutation Rates in Bacterial Populations. Methods **20:**4-17.
80. Alper H, Miyaoku K, Stephanopoulos G. 2005. Construction of lycopene-overproducing *E. coli* strains by combining systematic and combinatorial gene knockout targets. Nature Biotechnology **23:**612-616.
81. Wang HH, Isaacs FJ, Carr PA, Sun ZZ, Xu G, Forest CR, Church GM. 2009. Programming cells by multiplex genome engineering and accelerated evolution. Nature **460:**894-899.
82. Young RA. 2011. Control of the Embryonic Stem Cell State. Cell **144:**940-954.
83. Rider TH, Zook CE, Boettcher TL, Wich ST, Pancoast JS, Zusman BD. 2011. Broad-Spectrum Antiviral Therapeutics. *PLoS ONE* **6:**e22572.

84. Datsenko KA, Wanner BL. 2000. One-step inactivation of chromosomal genes in *Escherichia coli* K-12 using PCR products. Proc. Natl. Acad. Sci. USA **97:**6640-6645.
85. Jensen PD, Hammer K. 1998. The Sequence of Spacers between the Consensus Sequences Modulates the Strength of Prokaryotic Promoters. Applied and Environmental Microbiology **64:**82-87.
86. Kwok T, Yang J, Pittard AJ, Wilson TJ, Davidson BE. 1995. Analysis of an *Escherichia coli* mutant TyrR protein with impaired capacity for tyrosine mediated repression, but still able to activate at sigma 70 promoters. Molecular Microbiology **17:**471-481.
87. Koyanagi T, Katayama T, Suzuki H, Kumagai, H. 2008. Altered Oligomerization Properties of N316 Mutants of *Escherichia coli* TyrR. Journal of Bacteriology **190:**8238-8243.
88. Cui J, Somerville RL 1993. Mutational Uncoupling of the Transcriptional Activation Function of the TyrR Protein of *Escherichia coli* K-12 from the Repression Function. Journal of Bacteriology **175:**303-306.
89. Lawley B, Pittard AJ. 1994. Regulation of *aroL* Expression by TyrR Protein and Trp Repressor in *Escherichia coli* K-12. Journal of Bacteriology **176:**6921-6930.
90. Yang J, Wang P, Pittard AJ. 1999. Mechanism of Repression of the aroP P2 Promoter by the TyrR Protein of *Escherichia coli*. Journal of Bacteriology **181:**6411-6418.
91. Hall BM, Ma CX, Liang P, Singh KK. 2009. Fluctuation AnaLysis CalculatOR: a web tool for the determination of mutation rate using Luria-Delbrück fluctuation analysis. Bioinformatics **25:**1564-1565.
92. Kim SW, Keasling JD. 2001. Metabolic Engineering of the Nonmevalonate Isopentenyl Diphosphate Synthesis Pathway in *Escherichia coli* Enhances Lycopene Production. Biotechnology & Bioengineering **72:**408-415.
93. Jackel C, Kast P, Hilvert D. 2008. Protein Design by Directed Evolution. Annual Review Biophysics **37:**153-173.
94. Meinhold P, Peters MW, Hartwick A, Hernandez AR, Arnold FH. 2006. Engineering Cytochrom P450 BM3 for Terminal Alkane Hydroxylation. Adv. Synth. Catal. **348:**763-772.
95. Zurek G, Karst U. 1997. Microplate photometric determination of aldehydes in disinfectant solutions. Analytica Chimica Acta **351:**247-257.
96. Anthon GE, Barrett DM. 2004. Comparison of Three Colorimetric Reagents in the Determination of Methanol with Alcohol Oxidase. Application to the Assay of Pectin Methylesterase. Journal of Agricultural and Food Chemistry **52:**3749-3753.

Appendix A: Sequences

A.1. Sequences of primers (5' to 3') used to assemble plasmids in Chapter 2. Underlined parts indicate restriction sites unless otherwise indicated.

>HAD1-F
GGCCCATGGCAACCCCGCGTCAGATTCTTG
>HAD1-R
GGCGAATTCTTAACCGAGAAGGTCTTTTGC
>HAD2-F
GGCCCATGGGGTGCAAAGGTTTTCTGTTTG
>HAD2-R
GGCGAATTCTCACTGAATAATAACATCGCC
>HAD3-F
GGCCCATGGCCCGGATAGAAGCGGTATTTT
>HAD3-R
GGCGAATTCCTATGCCGTAATATCCCAACC
>HAD4-F
GGCCCATGGTCTATATCTTTGATTTAGGTA
>HAD4-R
GGCGAATTCTTAGCATAACACCTTCGCGAA
>HAD5-F
GGCCCATGGAGTGGGACTGGATTTTCTTTG
>HAD5-R
GGCGAATTCTCAGTGTTTACACAGGAGCTG
>HAD6-F
GGCCCATGGACGAGCGTTATGCAGGTTTAA
>HAD6-R
GGCGAATTCTCACAGCAAGCGAACATCCAC
>HAD7-F
GGCCCATGGCCGATTTACACACCGATGTAG
>HAD7-R
GGCGAATTCTTATTTCCCCCGTTTGGCGCG
>HAD8-F
GGCCCATGGATATCAACATTGCCTGGCAGG
>HAD8-R
GGCGAATTCTCACATTAGCGAGGGGATCAG
>HAD9-F
GGCCCATGGCTAACATTACCTGGTGCGACC
>HAD9-R
GGCGAATTCTTACTTCTGATTCAGGCTGCC
>HAD10-F
GGCCCATGGATAAGTTTGAAGATATTCGCG
>HAD10-R
GGCGAATTCTTAGTCATTTTTCGATTCCTG
>HAD11-F
GGCCCATGGAACTGCAAGGGGTAATTTTCG
>HAD11-R
GGCGAATTCCTATACGTTTTGCCAGAAGGC
>HAD12-F
GGCCCATGGGCGTAAAAGTTATCGTCACAG
>HAD12-R
GGCGAATTCTCAGCTGTTAAAAGGGGATGT
>HAD13-F

GGCCCATGGCTATTAAACTCATTGCTATCG
>HAD13-R
GGCGAATTCTTAATTCAGCACATACTTCTC
>HAD14-F
GGCCCATGGCCACACGCGTGATTGCTCTCG
>HAD14-R
GGCGAATTCTTAAATCAGGTGGCTATAAAT
>HAD15-F
GGCCCATGGGCATTAAATTAATTGCGGTAG
>HAD15-R
GGCGAATTCTTATTGGAGCCTGCGCGGTAT
>HAD16-F
GGCCCATGGACCAGGTTGTTGCGTCTGATT
>HAD16-R
GGCGAATTCTTACGATAAATAGAGTTTACG
>HAD17-F
GGCCCATGGCAGAACCGTTAACCGAAACCC
>HAD17-R
GGCGAATTCTTAGATACTACGACTAAACGA
>HAD18-F
GGCCCATGGCTCGTCTGGCAGCATTTGATA
>HAD18-R
GGCGAATTCTTATTCGGGGGAATAAGGTAG
>HAD19-F
GGCCCATGGTTTCAATTCAACAACCACTAC
>HAD19-R
GGCGAATTCTTAACGGGCGGAGAAAAAATG
>HAD20-F
GGCCCATGGCGAAGAGCGTACCCGCAATTT
>HAD20-R
GGCGAATTCTCATTGTGCCGGTTTTTGCTG
>HAD21-F
GGCCCATGGGTCAGAAGTATCTTTTTATCG
>HAD21-R
GGCGAATTCTTACAGCACTCCTTTCGACGA
>HAD22-F
GGCCCATGGGCAAAGCAGGTGCGTCGCTTG
>HAD22-R
GGCGAATTCTCATATCGATTGCCCTTTGGC
>HAD23-F
GGCCCATGGCCATTAAAAATGTAATTTGCG
>HAD23-R
GGCGAATTCTCAGATAACGTCGATTTCAGC
>NUDA-F
GGCCCATGGAAAAGCTGCAAATTGCGGTAG
>NUDA-R
GGCGAATTCCTACAGACGTTTAAGCTTCGC
>NUDB-F
GGCCCATGGAGGATAAAGTGTATAAGCG
>NUDB-R
GGCGAATTCTCAGGCAGCGTTAATTACAAACT
>NUDC-F
GGCCCATGGATCGTATAATTGAAAAATTAG
>NUDC-R
GGCGAATTCTCACTCATACTCTGCCCGACA
>NUDD-F

GGCCCATGGTTTTACGTCAGGAAGACTTTG
>NUDD-R
GGCGAATTCTCATAATCCGGGTACTCCGGT
>NUDE-F
GGCCCATGGGCAAATCATTACAAAAACCCA
>NUDE-R
GGCGAATTCTTACACTCGCCCCTGCCCTTT
>NUDF-F
GGCCCATGGTTAAGCCAGACAACCTGCCCG
>NUDF-R
GGCGAATTCTTATGCCCACTCATTTTTTAA
>NUDG-F
GGCCCATGGAAATGATTGAAGTTGTTGCCG
>NUDG-R
GGCGAATTCCTAATCCGCTGGTCTGGCGGC
>NUDH-F
GGCCCATGGTTGATGACGATGGCTACCGCC
>NUDH-R
GGCGAATTCTTAACCTCTTTTACGTCGATA
>NUDI-F
GGCCCATGGGACAACGGACTATTGTATGC
>NUDI-R
GGCGAATTCTTACAGAAGACCTTTCAAACG
>NUDJ-F
GGCCCATGGTTAAACCGCACGTTACCGTTG
>NUDJ-R
GGCGAATTCTTAGATGACACCCTTTGTAAA
>NUDK-F
GGCCCATGGCGCAACAAATCACCCTCATTA
>NUDK-R
GGCGAATTCTCAGTCCATTAAATGTGACGT
>NUDL-F
GGCCCATGGAATACCGTAGCCTGACGCTTG
>NUDL-R
GGCGAATTCTCAGGGTTTCACACCAATTTG
>NUDM-F
GGCCCATGGAACAGCGTCGTTTGGCAAGT
>NUDM-R
GGCGAATTCTCATTCTGCCGTTTCAGTCT
>NEMA-F
GGCGAATTCACCCGCGCTATCACAACAGTCTTAGCCCATTTTATGTCATCTGAAAAACTG
>NEMA-R
GGCGGTACCTTACAACGTCGGGTAATCGGT
>IDI-F
GGCGAATTCCGGGAGGAGGATTACTATATG
>IDI-R
GGCGGTACCTTATTTAAGCTGGGTAAATGCAG
>IDI-F2
GGCGAATTCATAAATCGAACACGTTTAGGAAGGAGCGCAACGATGCAAACGGAACACGTC
>IDI1-F
GGCGAATTCTAGCTTTCCCCGTCTACAATTTCTTCAAGATGACTGCCGACAACAAT
>IDI-NUDB-SOE-F
ACCGGTTCCACCACCACTACCGCCTCCACTTCCGCCACCTTTAAGCTGGGTAAATGC
>IDI-NUDB-SOE-R
AGTGGTGGTGGAACCGGTGGAGGCAGTGGTGGAGGCGTGAAGGATAAAGTG
>IDI1-NUDB-SOE-F

TCCACCGGTTCCACCACCACTACCGCCTCCTAGCATTCTATGAATTTG
>IDI1-NUDB-SOE-R
GGTGGTGGAACCGGTGGAGGCAGTGGTGGAGGCATGGAGGATAAAGTGTAT
>NUDB-R2
GGCGGTACCTCAGGCAGCGTTAATTAC
>NUDB-R3
GGCGGATCCGGCAGCGTTAATTACAAA
>NEMA-F2
GGCGGATCCTCACACAGGAAACAGACCATGTCATCTG
>NEMA-F3
GGCGGATCCGGAGGACAGCTAAATGTCATCTGAAAAACTGTA
>NEMA-R2
GGCTCTAGATTACAACGTCGGGTAATCGG

A.2. Sequences of primers (5' to 3') used to assemble plasmids in Chapter 4. Underlined parts indicate restriction sites unless otherwise indicated.

>Kan-F
GGCCCCGGGGTGTAGGCTGGAGCTGCTTC
>Kan-R
GGCGAGCTCATGGGAATTAGCCATGGTCC
>IdiKO-F
*ATCTATAATGATGAGTGATCAGAATTACATGTGAGAAATT*CCAGGCTTTACACTTTAT
>IdiKO-R
*TTACGTTATGCTCACAACCCCGGCAAATGTCGGGGTTTTT*ATGGGAATTAGCCATGGT
>DelHindIII-F
CAGGCATGCTTGCTTGGCTGTTTT
>DelHindIII-R
AAAACAGCCAAGCAAGCATGCCTG
>RFP-F
GGCGGTACCTTAAGTAGGGAGGTAAATACATGGTTTCCAAGGGCGAGGAG
>RFP-R
GGCTCTAGATTATTATTTGTACAGCTCATCCAT
>Idi-F
GGCAAGCTTATGCAAACGGAACACGTCATT
>Idi-SOE-R
ATGGAGCGACTCGTTAATTTTAAGCTGGGTAAATGC
>AraC-SOE-F
ATTAACGAGTCGCTCCATCCA
>AraC-R
GGCATCGATTTATGACAACTTGACGGCTAC
>AC-F
GGCAAGCTTATTAACGAGTCGCTCCATCCA
>I1I1-F
GGCGCTAGCCCAAAAAAACGGGTATGGAGAAACAGTAGAGAGTTGCGATAAAAAGCGTATG
GATAAAAATGCTAATCTTATGGATAAAAATGCTA
>I2I1-F
GGCGCTAGCCCAAAAAAACGGGTATGGAGAAACAGTAGAGAGTTGCGATAAAAAGCGTATG
GATAAAAATGCTAATCTTCAGGTAGGATCCGCTATGGCA
>I2I2-F
GGCGCTAGCCCAAAAAAACGGGTATGGAGAAACAGTAGAGAGTTGCGATAAAAAGCGTCAG
GTAGGATCCGCTAATCTTCAGGTAGGATCCGCTATGGCA
>AraReg-R
GGCAAGCTTCATACTCCCGCCATTCAG
>CFP-F
GGCATCGATTTTAAGAAGGAGATATACATATGACTA
>CFP-R
GGCTCCTGGACTATTATTTATACAGTTCATCCATGCC
>CP20-F
GGCCGCTAGCCATGGGTGAGTTTATTCTTGACAGTGCGGCCGGGGGCTGATATCATAGCAGAG
TACTATT CAATTTCACACAGGAAACAG AAGCTTGGCC
>CP20-R
GGCCAAGCTTCTGTTTCCTGTGTGAAATTGAATAGTACTCTGCTATGATATCAGCCCCCGGCCG
CACTGTCAAGAATAAACTCACCCATGGCTAGCGGCC
>TyrR-F
GGCAAGCTTATGCGTCTGGAAGTCTTTTGTGAA
>TyrR-R
GGCATCGATTTACTCTTCGTTCTTCTTCTGACT
>AroF0-F

GGCGCTAGCCTTTTTCAAAGCATAGCGGATTGT
>AroF0-R
GGCGAATTCGATGGCGATCCTGTTTATGCTCGT
>TyrR-E274Q-F
CGGTCGAGAGTCAGCTGTTTGGTC
>TyrR-E274Q-R
GACCAAACAGCTGACTCTCGACCG
>TyrR-N316K-F
TGCGTTTCCTTAAAGATGGCACTT
>TyrR-N316K-R
AAGTGCCATCTTTAAGGAAACGCA
>Del43TyrR-F
GGCAAGCTTATGTTTGCTGAACTGGAGTTTGAGAGT
>Del93TyrR-F
GGCAAGCTTATGGTGCTCTCTGTCGATATGAAAAGC
>Del187TyrR-F
GGCAAGCTTATGCGTATGGGCCGCCAGTTGCAAAAT
>AroL0-F
GGCGCTAGCGCGGAGCTGGAGAAGTGGTGGCTG
>AroL0-R
GGCGAATTCCGTGGGTTTTCCCCAATAGGTCGC
>AroLBox1and2-F
TATTGAGATTTTCACTTTATCGAAGTGGAATTTTTTCTTT
>AroLBox1and2-R
AAAGAAAAAATTCCACTTCGATAAAGTGAAAATCTCAATA
>AroLBox3-F
TCGTGGCTAAATATAATTTATTATTTATACTTCATTCTTG
>AroLBox3-R
CAAGAATGAAGTATAAATAATAAATTATATTTAGCCACGA
>AroP0-F
GGCGCTAGCACCGATTCACTTACCAATTTTGTG
>AroP0-R
GGCGAATTCGAAACCTCGTGCGGTGGTTGTTTT
>P2UP-F
AAGTCTTTTTGTTAACTTTCAAACTTCTTT
>P2UP-R
AAAGAAGTTTGAAAGTTAACAAAAAGACTT
>TEF-F
GGCGGATCCATAGCTTCAAAATGTTTCTAC
>TEF-R
GGCCCCGGGAAACTTAGATTAGATTGCTAT
>YEcitrine-F
GGCATCGATAACATGTCTAAAGGTGAAGAATTA
>YEcitrine-R
GGCAGATCTTTATTTGTACAATTCATCCATACC
>CYC1-SOE-F
GGCCTCGAGATCCGCTCTAACCGAAAAGGA
>CYC1-SOE-R
GTAGAAACATTTTGAAGCTATCTTCGAGCGTCCCAAAACCTT
>TEF-SOE-F
AAGGTTTTGGGACGCTCGAAGATAGCTTCAAAATGTTTCTAC
>TEF-SOE-R
GGCAAGCTTAAACTTAGATTAGATTGCTATGCT
>AD-F
GGCCCCGGGACCATGGCCAATTTTAATCAAAGTGGG
>AD-SOE-R

ACCGGTTCCACCACCACTACCGCCTCCACTTCCGCCACCCTCTTTTTTTGGGTTTGGTGG
>DBD-F
GGCAAGCTTACCATGAAGCTACTGTCTTCTATCGAA
>DBD-SOE-R
ACCGGTTCCACCACCACTACCGCCTCCACTTCCGCCACCCGATACAGTCAACTGTCTTTG
>GI-SOE-F
AGTGGTGGTGGAACCGGTGGAGGCAGTGGTGGAGGCCAAACGGAACACGTCATTTTATTG
>AD-GI-R
GGCCTCGAGTTATTTAAGCTGGGTAAATGCAGA
>DBD-GI-R
GGCGGTACCTTATTTAAGCTGGGTAAATGCAGA
>GI1-SOE-F
AGTGGTGGTGGAACCGGTGGAGGCAGTGGTGGAGGCACTGCCGACAACAATAGTATG
>AD-GI1-R
GGCCTCGAGTTATAGCATTCTATGAATTTGCCTG
>DBD-GI1-R
GGCGGTACCTTATAGCATTCTATGAATTTGCCTG
>GE20-SOE-F
AGTGGTGGTGGAACCGGTGGAGGCAGTGGTGGAGGCGCTTCAGAAAAAGAAATTAGGAGA
>AD-GE20-R
GGCCTCGAGCTATTTGCTTCTCTTGTAAACTTT
>DBD-GE20-R
GGCGGTACCCTATTTGCTTCTCTTGTAAACTTT
>DelHindIII-Erg20-F
GCTATCTACAAGCTATTGAAATCT
>DelHindIII-Erg20-R
AGATTTCAATAGCTTGTAGATAGC
>DelKpnI-Erg20-F
ACTGCTTCGGTACTCCAGAAC
>DelKpnI-Erg20-R
GTTCTGGAGTACCGAAGCAGT
>IA-StrepII-F
GGCGGTACCATGGCTGAAGCGCAAAATGATC
>IA-StrepII-R
GGCGGATCC*TCACTTTTCGAACTGCGGGTGGCTCCA*TGACAACTTGACGGCTACATC
>EMSA-AraReg-F
Cy5-AAGCTTCATACTCCCGCCATT
>EMSA-AraReg-R
GAATTCCTCCTGCTAGCCCAA
>EMSA-I1-F
Cy5-CACACTTTGCTATGCCATAGCATTTTTATCCATAAGAT
>EMSA-I1-R
ATCTTATGGATAAAAATGCTATGGCATAGCAAAGTGTG
>EMSA-I1I2-F
Cy5-TGCTATGCCATAGCATTTTTATCCATAAGATTAGCGGATCCTACCTGACGCTTTTTATCG
>EMSA-I1I2-R
CGATAAAAAGCGTCAGGTAGGATCCGCTAATCTTATGGATAAAAATGCTATGGCATAGCA
>I1-1F
FL-CACACTTTGCTATGCCATAGC
>I1-2F
ATTTTTATCCATAAGAT
>I1-3R
ATCTTATGGATAAAAATGCTA-BQ
>I1-4R
TGGCATAGCAAAGTGTG
>I1I2-1F

FL-TGCTATGCCATAGCATTTTTATCCATAAGAT
>I1 I2-2F
TAGCGGATCCTACCTGACGCTTTTTAT
>I1 I2-3R
ATAAAAAGCGTCAGGTAGGATCCGCTAATCT-BQ
>I1 I2-4R
TATGGATAAAAATGCTATGGCATAGCA
>MutD-F
GGCGAATTCTTTAAGAAGGAGATATACATATGA
>MutD-R
GGCGGTACCTTATGCTCGCCAGAGGCAACTTCC

Appendix B: Tables

B.1. Strains and plasmids used in Chapter 2.

Name	Archive #	Description
pHAD1	JBEI-4498	HAD1
pHAD2	JBEI-4499	HAD2
pHAD3	JBEI-4500	HAD3
pHAD4	JBEI-4501	HAD4
pHAD5	JBEI-4502	HAD5
pHAD6	JBEI-4503	HAD6
pHAD7	JBEI-4504	HAD7
pHAD8	JBEI-4505	HAD8
pHAD9	JBEI-4506	HAD9
pHAD10	JBEI-4507	HAD10
pHAD11	JBEI-4508	HAD11
pHAD12	JBEI-4509	HAD12
pHAD13	JBEI-4510	HAD13
pHAD14	JBEI-4511	HAD14
pHAD15	JBEI-4512	HAD15
pHAD16	JBEI-4513	HAD16
pHAD17	JBEI-4514	HAD17
pHAD18	JBEI-4515	HAD18
pHAD19	JBEI-4516	HAD19
pHAD20	JBEI-4517	HAD20
pHAD21	JBEI-4518	HAD21
pHAD22	JBEI-4519	HAD22
pHAD23	JBEI-4572	HAD23
pNudA	JBEI-4573	NudA
pNudB	JBEI-4574	NudB
pNudC	JBEI-4575	NudC
pNudD	JBEI-4576	NudD
pNudE	JBEI-4577	NudE
pNudF	JBEI-4578	NudF
pNudG	JBEI-4579	NudG
pNudH	JBEI-4580	NudH
pNudI	JBEI-4581	NudI
pNudJ	JBEI-4582	NudJ
pNudK	JBEI-4583	NudK
pNudL	JBEI-4584	NudL
pNudM	JBEI-4585	NudM
pPro29b-NudB	JBEI-4586	NudB with 5’ S-tag and 3’ His-tag
pIdi	JBEI-4587	Idi
pNudB-s-Idi	JBEI-4588	NudB and Idi
pIdi-NudB	JBEI-4589	Idi-NudB fusion
pIdi1-NudB	JBEI-4590	Idi1-NudB fusion
pNemA	JBEI-4591	NemA
pIdi-NudB-s-NemA	JBEI-4592	Idi-NudB fusion and NemA
pIdi1-NudB-s-NemA	JBEI-4593	Idi1-NudB fusion and NemA

B.2. Strains and plasmids used in Chapter 4.

Name	Archive #	Description
HC175	JBEI-4442	E. coli MG1655 Δ*idi*::(P_{lac} *mk pmk pmd kan*)
DJ106	JBEI-4443	*E. coli* BLR *ΔtyrR*
DJ166	JBEI-4444	*E. coli* BLR *ΔtyrR ΔpheA/L aroF*[P124L] *tyrA*[M53I; A354V]
DJ238	JBEI-4445	*E. coli* MG1655 *ΔtyrR*
MO219	JBEI-4446	EPY219 (*27*) without pADS
pLyc	JBEI-4447	Lycopene expression plasmid
pCtl-RFP-S_{AraC}	JBEI-4448	AraC sensor with RFP and *mutD*
pCtl-RFP-S_{IA}	JBEI-4449	IA sensor with RFP and *mutD*
pCtl-RFP-S_{AC}	JBEI-4450	AC sensor with RFP and *mutD*
pCtl-RFP-S_{IA32}	JBEI-4451	IA32 sensor with RFP and *mutD*
pCtl-S_{IA44}	JBEI-4452	IA44 sensor with *mutD*
pCtl-RFP-S_{IA44}	JBEI-4453	IA44 sensor with RFP and *mutD*
pCtl-RFP-S_{IA}-I1I1	JBEI-4454	IA sensor with RFP, I_1I_1, and *mutD*
pCtl-RFP-S_{IA}-I2I1	JBEI-4455	IA sensor with RFP, I_2I_1, and *mutD*
pCtl-RFP-S_{IA}-I2I2	JBEI-4456	IA sensor with RFP, I_2I_2, and *mutD*
pCtl-CFP-RFP-S_{AC}	JBEI-4457	AC sensor with RFP, CFP, and *mutD*
pCtl-CFP-RFP-S_{AraC}	JBEI-4458	AraC sensor with RFP, CFP, and *mutD*
pCtl-CFP-RFP-S_{IA}	JBEI-4459	IA sensor with RFP, CFP, and *mutD*
pCtl-RFP-S_{aroF0}	JBEI-4460	aroF0 sensor with RFP
pCtl-RFP-S_{aroF1}	JBEI-4461	aroF1 sensor with RFP
pCtl-RFP-S_{aroF2}	JBEI-4462	aroF2 sensor with RFP
pCtl-RFP-S_{aroF3}	JBEI-4463	aroF3 sensor with RFP
pCtl-RFP-S_{aroF4}	JBEI-4464	aroF4 sensor with RFP
pCtl-RFP-S_{aroF5}	JBEI-4465	aroF5 sensor with RFP
pCtl-RFP-S_{aroF6}	JBEI-4466	aroF6 sensor with RFP
pCtl-RFP-S_{aroL0}	JBEI-4467	aroL0 sensor with RFP
pCtl-RFP-S_{aroL1}	JBEI-4468	aroL1 sensor with RFP
pCtl-RFP-S_{aroL2}	JBEI-4469	aroL2 sensor with RFP
pCtl-RFP-S_{aroL3}	JBEI-4470	aroL3 sensor with RFP
pCtl-RFP-S_{aroL4}	JBEI-4471	aroL4 sensor with RFP
pCtl-RFP-S_{aroL5}	JBEI-4472	aroL5 sensor with RFP
pCtl-RFP-S_{aroP0}	JBEI-4473	aroP0 sensor with RFP
pCtl-RFP-S_{aroP1}	JBEI-4474	aroP1 sensor with RFP
pCtl-RFP-S_{aroP2}	JBEI-4475	aroP2 sensor with RFP
pCtl-RFP-S_{aroP3}	JBEI-4476	aroP3 sensor with RFP
pCtl-RFP-S_{aroP4}	JBEI-4477	aroP4 sensor with RFP
pCtl-RFP-S_{aroP5}	JBEI-4478	aroP5 sensor with RFP
pCtl-RFP-S_{aroP6}	JBEI-4479	aroP6 sensor with RFP
pESC-YFP-P_{TEF}	JBEI-4480	Yeast expression plasmid without any sensors
pESC-YFP-$S_{Idi\text{-}GAL4}$	JBEI-4481	Idi-GAL4 sensor with YFP
pESC-YFP-$S_{Idi1\text{-}GAL4}$	JBEI-4482	Idi1-GAL4 sensor with YFP
pESC-YFP-$S_{Erg20\text{-}GAL4}$	JBEI-4483	Erg20-GAL4 sensor with YFP
pPro29b-IA	JBEI-4484	IA tagged with Strep-tag II

pMut-S_{AC}	JBEI-4485	AC sensor with *mutD5*
pMut-S_{IA44}	JBEI-4486	IA44 sensor with *mutD5*
pMut-S_{IA32}	JBEI-4487	IA32 sensor with *mutD5*
pMut-S_{AraC}	JBEI-4488	AraC sensor with *mutD5*
pMut-RFP-S_{IA44}	JBEI-4489	IA44 sensor with *mutD5* and RFP
pMut-RFP-S_{AraC}	JBEI-4490	AraC sensor with *mutD5* and RFP
pMut-RFP-S_{aroF3}	JBEI-4491	aroF3 sensor with *mutD5* and RFP
HC229	JBEI-4492	*E. coli* undergoing FREP using IA44 with pLyc after 72 hrs
HC230	JBEI-4493	*E. coli* undergoing FREP using IA44 with pLyc after 144 hrs
HC231	JBEI-4494	*E. coli* undergoing FREP using IA44 with pLyc after 216 hrs
HC232	JBEI-4495	*E. coli* undergoing FREP using IA44 with pLyc after 288 hrs
HC233	JBEI-4496	*E. coli* undergoing FREP using IA44 with pLyc after 360 hrs
HC234	JBEI-4497	*E. coli* undergoing FREP using IA44 with pLyc after 432 hrs